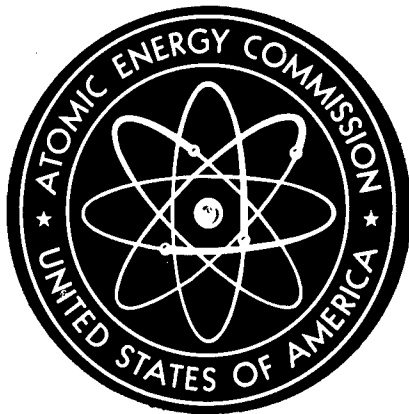


B4



HASL-195

THE RADIATION FIELD IN AIR  
DUE TO DISTRIBUTED GAMMA-RAY  
SOURCES IN THE GROUND

By

H. Beck  
G. de Planque

**DISTRIBUTION STATEMENT A**  
Approved for Public Release  
Distribution Unlimited

May 1968

DATA QUALITY INDICATED 4

20000914 120

Reproduced From  
Best Available Copy

## LEGAL NOTICE

This report was prepared as an account of Government sponsored work. Neither the United States, nor the Commission, nor any person acting on behalf of the Commission:

A. Makes any warranty or representation, expressed or implied, with respect to the accuracy, completeness, or usefulness of the information contained in this report, or that the use of any information, apparatus, method, or process disclosed in this report may not infringe privately owned rights; or

B. Assumes any liabilities with respect to the use of, or for damages resulting from the use of any information, apparatus, method, or process disclosed in this report.

As used in the above, "person acting on behalf of the Commission" includes any employee or contractor of the Commission, or employee of such contractor, to the extent that such employee or contractor of the Commission, or employee of such contractor prepares, disseminates, or provides access to, any information pursuant to his employment or contract with the Commission, or his employment with such contractor.

This report has been reproduced directly from the best available copy.

Printed in USA. Price \$3.00 Available from the Clearing-house for Federal Scientific and Technical Information, National Bureau of Standards, U. S. Department of Commerce, Springfield, Virginia 22151.

HASL-195  
HEALTH AND SAFETY (TID-4500)

THE RADIATION FIELD IN AIR DUE TO DISTRIBUTED GAMMA-RAY  
SOURCES IN THE GROUND

H. Beck  
G. de Planque

May 1968

Health and Safety Laboratory  
U. S. Atomic Energy Commission  
New York, New York

---

## ABSTRACT

A much more complete and detailed picture of the external environmental  $\gamma$ -ray radiation field has been obtained through  $\gamma$ -ray transport calculations of exposure rates, differential energy spectra, integral exposure rate spectra, and angular exposure rate distributions due to sources distributed on or in the soil half space.

The radiation field is examined not only for the natural emitters  $^{40}\text{K}$ ,  $^{238}\text{U}$ , and  $^{232}\text{Th}$  but also for  $\gamma$ -rays whose energies are typical of weapons test fallout. The energy spectra and exposure rate angular distributions are shown to vary with detector height and source distribution with resulting important implications in regard to detector calibration and prediction of ground level exposure rates from aerial survey data.

Exposure rate results as a function of detector height in air above the soil air interface are tabulated for various source energies and source distributions. Although the calculated results are for specific soil and air densities, soil moisture and composition, the data can easily be adapted to other soil and air conditions.

---

## TABLE OF CONTENTS

	<u>Page</u>
TEXT	
I. Introduction.....	1
II. Adaptation of the Polynomial Expansion Matrix Equation Method to the Air-Soil Interface Problem..	3
A. Exposure Rate Dependence on Soil Density.....	3
B. Exposure Rate Dependence on Air Density.....	5
C. Exposure Rate Dependence on Soil Composition and Moisture Content.....	5
D. Error Estimates.....	6
III. Radiation in Air Due to the Uniformly Distributed Naturally Occurring Sources in the Soil.....	8
A. Exposure Rates.....	9
B. Differential Energy Spectra.....	10
C. Integral Exposure Rate Spectra.....	11
D. Differential Angular Exposure Rates.....	12
IV. Radiation in Air Due to Exponentially Distributed (Fallout) Sources in the Soil.....	14
A. Exposure Rates.....	15
B. Differential Energy Spectra.....	17
C. Integral Exposure Spectra.....	17
D. Angular Distributions.....	17
V. Conclusions.....	19
References.....	20

TABLE OF CONTENTS (Cont'd)

TABLES

	<u>Page</u>
<b>Table 1. Source Spectra Used for <math>^{238}\text{U}</math> and <math>^{232}\text{Th}</math> Exposure Rate Calculations.....</b>	22
<b>Table 2. Exposure Rates - Uniformly Distributed Source..</b>	23
A. Total Exposure Rate.....	23
B. Unscattered $\gamma$ -Rays.....	24
<b>Table 3. Exposure Rates in Air Due to <math>^{40}\text{K}</math>, <math>^{238}\text{U}</math>, and <math>^{232}\text{Th}</math> in the Soil (<math>\mu\text{r}/\text{hr}</math>).....</b>	25
<b>Table 4. Percentage of Total Exposure Rate Due to Skyshine for Uniformly Distributed Sources.....</b>	26
<b>Table 5. Exposure Rates - Exponentially Distributed Source.....</b>	27
A. Total Exposure Rate.....	27
B. Unscattered $\gamma$ -Rays.....	31
<b>Table 6. Percentage of Total Exposure Rate Due to Skyshine-Exponentially Distributed Sources.....</b>	34

ILLUSTRATIONS

<b>Figure 1. Total and scattered exposure rates as a function of height for uniformly distributed sources.....</b>	35
<b>Figure 2. Differential energy spectra of the scattered energy flux for soil-air and infinite air media.....</b>	36
<b>Figure 3. Integral exposure rate spectra for uniformly distributed sources.....</b>	37

TABLE OF CONTENTS (Cont'd)

	<u>Page</u>
Figure 4. Integral exposure rate spectra for the natural emitters.....	38
Figure 5. Differential angular exposure rate distributions of scattered and unscattered $\gamma$ -rays for uniformly distributed sources.....	39
Figure 6. Differential angular exposure rate distributions of unscattered $\gamma$ -rays for uniformly distributed sources.....	40
Figure 7. Differential angular exposure rate distribution for the natural emitters.....	41
Figure 8. Total exposure rates as a function of height for exponentially distributed sources.....	42
Figure 9. Total exposure rates as a function of height for plane sources.....	43
Figure 10. Total and scattered exposure rates as a function of height for various exponentially distributed sources.....	44
Figure 11. Total exposure rates as a function of energy for various exponentially distributed sources..	45
Figure 12. Effect of source depth distribution on total exposure rates at various heights relative to the total exposure rates at 1 meter.....	46
Figure 13. The ratio of the exposure rate due to scattered $\gamma$ -rays to the total exposure rate as a function of source energy for various depth distributions.....	47

TABLE OF CONTENTS (Cont'd)

	<u>Page</u>
Figure 14. Differential energy spectra of the scattered energy flux for a .662 MeV source....	48
Figure 15. Integral exposure rate spectra for a .364 MeV source.....	49
Figure 16. Integral exposure rate spectra for a .662 MeV source.....	50
Figure 17. Integral exposure rate spectra for a 1.25 MeV source.....	51
Figure 18a and 18b. Differential angular exposure rate distributions for plane and exponentially distributed sources....	52,53

## I. INTRODUCTION

A knowledge of the radiation field in air due to  $\gamma$ -ray emitters distributed in the soil is important for estimating exposure rates from a given source concentration, evaluating hazards to the population, and properly interpreting and relating radiation measurements made at ground level and at airplane altitudes. The sources of this radiation are the naturally occurring radioisotopes, fallout from nuclear weapons tests, or unanticipated releases into the environment from a nuclear reactor installation.

The calculation of the exposure rate in air due to these sources in the soil has usually been based on infinite medium buildup factors. The exposure rate from a distributed source in the soil was usually calculated by assuming a single medium composition, either all air if the sources were distributed close to the interface or all soil (aluminum was usually substituted for soil) if the sources were distributed throughout the soil half space. The easily computed direct beam exposure rate for each point source element in the chosen medium was multiplied by the appropriate buildup factor and an integration performed numerically (or analytically by substituting a functional fit to the buildup factor data) to obtain the total exposure rate<sup>(1)</sup>. This rough solution was necessary because of the lack of analytical transport methods for solving the one-dimensional two-media  $\gamma$ -ray transport problem. The infinite medium buildup factor approach, besides failing to account for the differences in the transport properties of soil and air at low energies, provided no information on the energy and angle distribution of the  $\gamma$ -rays entering the detector; information important for interpreting field measurements.

In this report, we present accurate calculations of  $\gamma$ -ray exposure rates in air (better than  $\pm 5\%$  S.D.) for source distributions characteristic of natural and fallout  $\gamma$ -ray emitters in the soil as well as differential energy spectra,

integral exposure rate spectra, and exposure rate angular distributions heretofore not available. In addition, we discuss sensitivity of the data to source energy, source depth distribution in the soil, and detector height above the interface. The calculations were carried out using a combination of the P-3 and DP-1 polynomial expansion matrix equation method for solving the two media transport problem<sup>(2)</sup>. Comparison of these results with those obtained using the infinite medium moments method based on buildup factors indicated that the latter method was probably fairly accurate ( $\pm 10\%$ ) for detector positions close to the interface but may have been significantly in error far from the interface, especially for low energy sources distributed in the soil<sup>(2)</sup>.

In addition to the specific calculations of the differential energy spectra, integral exposure rate spectra, and exposure rate angular distributions, the effects of varying the soil composition, moisture content, and density are considered together with an evaluation of the calculational accuracy.

---

## II. ADAPTATION OF THE POLYNOMIAL EXPANSION MATRIX EQUATION METHOD TO THE AIR-SOIL INTERFACE PROBLEM

Calculational details for solving the two media transport problem by the P-3 and DP-1 polynomial expansion matrix equation method appear in a previous report<sup>(2)</sup>. In general, the method consists of separating the spatial and angular dependencies of the angular flux in a truncated series of orthogonal polynomials and making use of the orthogonality properties to reduce the Boltzmann equation to a set of coupled integro-differential equations for each spatial component of the flux. These equations are solved by dividing the energy range into a number of groups and replacing the integration over energy by a summation over these groups. The integro-differential equations are rewritten as a set of differential matrix equations<sup>(3)</sup>. These equations have relatively simple exponential solutions. The solution for a given energy group constitutes the source term for the next lower group. Thus, starting at the source energy, the differential energy and angle spectrum can be constructed stepwise down to any desired energy. Total exposure rates and angular exposure rates are obtained by weighting the differential spectra by the appropriate energy absorption coefficient and integrating over the energy and angular intervals of interest. All cross section data used for these calculations were taken from Hubbell<sup>(4)</sup>.

The calculations discussed in this report are for a given set of soil and air densities, soil moisture content, and soil composition. However, as this section points out, our data can be applied to other soil and air conditions.

### A. Exposure Rate Dependence on Soil Density

The calculated exposure rates are for a soil in situ density of 1.6 gm/cm<sup>3</sup>. Actual in situ densities of soils can range from less than 1.0 gm/cm<sup>3</sup> to over 2.0 gm/cm<sup>3</sup>, although a typical range<sup>(5)</sup> would be 1.1 to 1.8 gm/cm<sup>3</sup>.

Since in our calculations we are dealing with a one-dimensional medium in the sense that only the direction perpendicular to the soil-air interface enters into the  $\gamma$ -ray transport equation and then only in terms of the  $\gamma$ -ray mean free path (mfp), the effect of changing the soil density is equivalent to a changing scale factor in this direction. This is because the  $\gamma$ -ray mean free path is equal to the inverse of the total attenuation coefficient, a quantity directly proportional to the density of the medium. Therefore, the soil density can affect calculations with certain source distributions.

For a source distributed exponentially with depth ( $S = S_0 e^{-\alpha z}$ , where  $S$  is the activity at depth  $z$ ,  $S_0$  is the surface activity, and  $\alpha$  is the reciprocal of the relaxation length), changing the density,  $\rho$ , is equivalent to changing the effective source distribution such that  $\alpha' = 1.6 \alpha/\rho$ . (In each case the total source activity in a 1 cm<sup>3</sup> column = 1  $\gamma/\text{sec}$ ). Thus, increasing the soil density effectively buries the source more deeply, decreasing the flux and exposure rate at the detector in the air half space. Therefore, in order to use the data given at certain relaxation lengths in this report for a density other than 1.6 gm/cm<sup>3</sup>, one would have to apply the above transform,  $\alpha' = 1.6 \alpha/\rho'$ , to determine which relaxation length to use. Since  $\alpha \rightarrow \infty$  corresponds to an infinite plane source it follows that the soil density has no effect for this case.

When our calculations are for a uniformly distributed source of one  $\gamma$ -ray emitted per cm<sup>3</sup> at 1.6 gm/cm<sup>3</sup>, the calculated exposures and fluxes are valid for a uniformly distributed source of intensity  $1.6/\rho$  gammas emitted/cm<sup>3</sup>-sec where  $\rho$  is the actual in situ soil density. This is so because changing the density by some factor is equivalent to changing the source intensity in the mean free path interval ( $dt$ , which is  $t$  mfp from the interface) by this same factor.

B. Exposure Rate Dependence on Air Density

The air density used in our calculations was  $1.204 \text{ mg/cm}^3$  corresponding to a temperature of  $20^\circ\text{C}$ . Since  $\gamma$ -ray distances must be measured in mean free paths, the fluxes and exposures for other air densities can be obtained through adjustments to our data as in the case of differing soil densities. Thus, our data at  $h$  meters represents the flux or exposure rate at a distance  $(1.204 \times 10^{-3}/\rho')h$  where  $\rho'$  is the new air density.

C. Exposure Rate Dependence on Soil Composition and Moisture Content

In our calculations, the assumed soil constituent concentrations given in percentage of total weight were  $\text{SiO}_2 - 67.5\%$ ,  $\text{Al}_2\text{O}_3 - 13.5\%$ ,  $\text{Fe}_2\text{O}_3 - 4.5\%$ ,  $\text{CO}_2 - 4.5\%$ , and  $\text{H}_2\text{O} - 10.0\%$ .

Changing the composition of the soil medium affects the fluxes and exposures more fundamentally than changes in density since Compton scattering, which is the dominant process at the higher energies, is proportional to the average  $Z/A$  of the soil while photoelectric absorption, which dominates at low energies, depends on the atomic number  $Z$ . Thus, a soil with more water in it would have an increased  $Z/A$  due to the lesser number of electrons per hydrogen atom as compared to most of the other soil constituents and, therefore, relatively more Compton scattering.

High  $Z$  materials in the soil such as iron could also affect the exposure rates and spectra. We investigated this possible dependence on soil composition by comparing calculations for our standard mock soil which has an average  $(Z/A)$  of .503 with similar calculations for pure aluminum having a  $(Z/A)$  of .482, a range of  $(Z/A)$  typical of most soils. Relatively minor differences were found in the exposure rates calculated for these two materials indicating that the radiation field is not extremely sensitive to the exact composition of the soil. For a .662 MeV plane source

distributed on the interface, the differences for both the unscattered and total exposure rates at  $h = 1$  meter were less than 1%, while at  $h = 100$  meters, the differences were less than 0.5%. The differences were slightly larger when the source was distributed in the soil. For a uniformly distributed 1.0 MeV source, the unscattered aluminum exposure rate was found to be about 4% greater than the corresponding soil value at  $h = 1$  meter and about 3.5% greater at  $h = 100$  meters. The total exposure rates were 3.4% greater for aluminum than for soil at both heights.

A further comparison was made by calculating the exposure rates for soils whose ratios of constituents other than water were the same as our mock soil, but whose moisture contents were 0% and 25% as compared to the 10% of our standard soil. In all cases the density was kept constant at  $1.6 \text{ gm/cm}^3$  and the source was 1.0 MeV, uniformly distributed, since the aluminum calculations indicated the greatest differences occur for a distributed source. The 0% and 10% moisture soils gave almost identical results while the 25% moisture soil gave exposure rates only 1.7% lower than the 10% moisture soil at both 1 meter and 100 meters. This small difference is in the direction expected since the increased moisture content would cause slightly more Compton scattering relative to photoelectric absorption. The  $(Z/A)$  for the 0% moisture content soil was .497, while the  $(Z/A)$  for the 25% case was .512.

Thus, the calculations are relatively insensitive to minor differences in soil composition and moisture content and should be valid for a wide range of soils. Corrections would, of course, have to be made when the density changes due to rainfall. These corrections are discussed under Section II, A.

#### D. Error Estimates

Exposure rates, in this report, are given in units of  $\text{MeV/gm-sec}$  and represent the energy absorbed in a gram of

air, per unit time, i.e. the flux weighted by the photon energy and mass energy transport coefficient for air. The flux was calculated down to a low energy cutoff of  $\tau_0 + 13.2$  ( $\tau_0 = \frac{511}{E}$ ). This low energy cutoff has been found to include over 99% of the energy except for the highest energies and for very large interface to detector distances. For these latter cases a correction was made by interpolating the differential energy spectrum down to lower energies. For all calculations, annihilation radiation, bremsstrahlung, and coherent scattering were neglected.

The polynomial expansion method can be expected to provide exposure rate estimates for scattered  $\gamma$ -rays of accuracy better than 5%<sup>(2)</sup>. In many cases the scattered component is smaller than the unscattered component. The latter was calculated exactly and any error in it is due only to errors in the cross section data. Thus, the error in the total exposure rate is smaller than the error in the scattered component. To improve the calculational procedure, the values of the differential scattered flux and the exposure rate at the source energy were calculated directly using an exact expression. Inasmuch as the  $\gamma$ -ray cross section data are felt to be quite accurate (better than 2%) for the source energies and media used in our calculations, we conclude that the error in exposure rate values as well as in the differential energy spectra and the integral exposure rate spectra is always less than  $\pm 5\%$ . The angular distributions are not as accurate and the error here may be as much as  $\pm 10\%$  or more for the scattered component when the detector is near the interface<sup>(2)</sup>.

### III. RADIATION IN AIR DUE TO THE UNIFORMLY DISTRIBUTED NATURALLY OCCURRING SOURCES IN THE SOIL

Gamma radiation in air due to naturally occurring isotopes in the soil is usually calculated by assuming uniform distribution in the soil. The only natural emitters of consequence are  $^{40}\text{K}$ ,  $^{238}\text{U}$ , and  $^{232}\text{Th}$ . The latter two isotopes decay by means of a long chain process and  $^{40}\text{K}$  decays to  $^{40}\text{A}$  with the emission of a single 1.46 MeV  $\gamma$ -ray. For the  $^{238}\text{U}$  series, most of the  $\gamma$ -rays are emitted by RaC ( $^{214}\text{Bi}$ ) and RaB ( $^{214}\text{Pb}$ ) which are daughters of  $^{222}\text{Rn}$ , a gaseous daughter of  $^{226}\text{Ra}$ . Because it is a gas,  $^{222}\text{Rn}$  can emanate from soil particles, diffuse through the soil air to the surface and escape into the atmosphere. This effect tends to reduce the  $\gamma$ -ray emission in the soil due to  $^{238}\text{U}$  by as much as 50%, thus lessening the importance of the  $^{238}\text{U}$  series relative to the other two emitters<sup>(1)</sup>. The  $^{232}\text{Th}$  series contributes a large number of  $\gamma$ -rays of varying energies from several different daughter isotopes. Although one of these emitters is a gas, thoron ( $^{220}\text{Rn}$ ), the short half life of this isotope (54.5 sec) prevents any significant escape and subsequent loss of soil gamma activity.

Since the decay schemes of  $^{226}\text{Ra}$  and  $^{232}\text{Th}$  (particularly the relative intensities of the various decay levels) are still somewhat uncertain, we give in Table 1 the source spectra and intensities used for the calculations in this report. These energies and intensities are our estimates based on the best available data. Some of the weaker energy lines have been grouped together or included with stronger lines in order to keep the total number of source energies manageable.

Table 2 gives the exposure rates for monoenergetic sources ranging from 0.25 to 2.75 MeV vs. detector height so that if necessary the reader can recalculate  $^{238}\text{U}$  and  $^{232}\text{Th}$  exposure rates for other source spectra. The  $^{238}\text{U}$

and  $^{232}\text{Th}$  exposure rates were obtained by interpolating from the data in Table 2 for the source energies in Table 1, multiplying by the number of  $\gamma$ -rays emitted per  $^{238}\text{U}$  and  $^{232}\text{Th}$  disintegration and summing.

Calculations of the exposure rates for uniformly distributed sources in the soil are discussed and evaluated together with the differential energy spectra, integral exposure rate spectra, and angular exposure rates.

#### A. Exposure Rates

The total exposure rates as well as the direct beam or unscattered component are given in Table 2 as functions of source energy for various detector heights. Figure 1 illustrates the variation of exposure rates with height for three different source energies. Note that the total exposure rate changes very little in the first 10 meters above the interface but then begins to drop off fairly rapidly with height with the lower energy sources falling more rapidly than the higher energy sources due in large part to the more rapid decrease of the unscattered component for low source energies. The scattered components fall off less rapidly than the total exposure rate. Since the calculated exposure rates for  $^{40}\text{K}$ ,  $^{238}\text{U}$  series, and the  $^{232}\text{Th}$  series all showed almost exactly the same variation with height even though their source spectra varied considerably (Table 3), a single curve is given in Figure 1 for the variation with height of the natural gamma emitters.

The variation with height of the natural emitter exposure rate, given in Figure 1, was crudely verified by us at a single location by making ionization chamber measurements at  $h = 1$  meter and  $h = 7$  meters above a predominantly (95%) natural  $\gamma$ -radiation field. The measured variation in exposure rate with height of 14% compares reasonably well with the 11% reduction predicted by Figure 1, and is within the experimental error.

Our previous calculations of  $^{238}\text{U}$ ,  $^{232}\text{Th}$  and  $^{40}\text{K}$  exposure rates based on the infinite medium buildup factors are also given in Table 3. These calculations for an infinite medium assumed that the energy absorbed at the earth-air interface per gram of air would be  $\frac{1}{2}$  the energy emitted per gram of soil<sup>(1)</sup>. Since for low energies the absorption in soil is greater than in air this tended to overestimate the exposure rate. By comparing the  $^{40}\text{K}$  results (Table 3), we see that this overestimate was only about 4% for 1.46 MeV. It would have been greater for a lower energy source. The much larger differences in the old and new calculated  $^{238}\text{U}$  exposure rates, however, are due not as much to the more accurate method (which accounts for only about 5-8% of the difference) as to the different source relative intensities used in the present work. In any case, the small changes in the values of  $^{238}\text{U}$ ,  $^{232}\text{Th}$  and  $^{40}\text{K}$  exposure rates per unit concentration of these elements do not significantly alter any of the results given in any of our previous reports on environmental radiation<sup>(1,6)</sup>.

The present report, of course, is much more detailed than our previous work, since it provides data on energy and angle distributions and detector height dependence rather than just exposure rates at one meter above the interface.

#### B. Differential Energy Spectra

The relative contributions of various energy photons to the total scattered energy spectrum is determined by examining the differential energy spectra. The differential energy spectra of the scattered energy flux (flux x energy) for three source energies, .364 MeV, 1.0 MeV, and 2.5 MeV are shown in Figure 2 for  $h = 1.0$  meter and  $h = 100$  meters. The effect of the increased scattering in air relative to soil at the lower energies is illustrated in the figure by the shift to lower energy and buildup of the Compton peak

at around 50-100 keV as the detector height is increased. The relatively high photoelectric cross section in soil compared to air causes it to act as a sink for low energy  $\gamma$ -rays, an effect which is enhanced the lower the source energy. To further illustrate the magnitude of this effect, we have also shown in Figure 2 the spectrum for a 1 MeV source at 1 meter in an infinite air medium instead of a soil-air medium. For this source energy the difference in the total exposure rate is only about 5% in all since about 50% of the exposure rate is due to unscattered  $\gamma$ -rays. At lower source energies, where the scattered  $\gamma$ -rays contribute a larger portion of the total exposure rate, the effect on the total exposure rate of using infinite air calculations would be more significant.

### C. Integral Exposure Rate Spectra

Another way to examine the effect of different regions of the energy spectrum on the total exposure rate is to examine the integral exposure rate spectrum, i.e. the fraction of the total exposure rate due to  $\gamma$ -rays of energy less than E. This approach can be extended easily to the analysis of the composite  $^{238}\text{U}$  and  $^{232}\text{Th}$  spectra. Figure 3 illustrates that as the detector height increases the fraction of the total exposure rate due to low energy photons increases. The effect is more pronounced the lower the initial source energy since the percentage of unscattered  $\gamma$ -rays is lower and the fractional change in energy due to a collision is smaller. For the 2.5 MeV source only 2% of the exposure rate is from  $\gamma$ -rays of less than 100 keV at h = 1 meter and only 5% at h = 100 meters, while for a .364 MeV source, the corresponding values are 13% and 30%. The values at the source energy in Figure 3 indicate the fraction of the exposure rate due to scattered  $\gamma$ -rays. This fraction, of course, decreases with increasing energy.

Figure 4 shows the integral spectra for  $^{40}\text{K}$ ,  $^{238}\text{U}$  series and  $^{232}\text{Th}$  series. The U and Th spectra are quite similar.

The curves which represent the results at 100 meters illustrate the softening of the spectral composition of the radiation with height. The  $^{40}\text{K}$  spectrum at 1 meter is quite a bit harder than the  $^{238}\text{U}$  and  $^{232}\text{Th}$  spectra but as the detector height is increased this difference becomes smaller since the higher energy sources in the  $^{238}\text{U}$  and  $^{232}\text{Th}$  series dominate resulting in a lesser overall rate of softening as compared to that for the single 1.46 MeV  $^{40}\text{K}$  source. Figure 4 indicates, however, that the fraction of the exposure rate due to photons of less than 200 keV can become quite significant as the detector height is increased, depending on the source. Since many detectors used in the field have an energy dependence different from that of air at low energies, it may be inappropriate to use the same calibration factors for these instruments at different heights above the interface. This would be especially true for an instrument calibrated in terms of photon number per unit time such as a scintillation counter since a large increase in the exposure rate due to low energy photons would result in an even larger increase in the actual number of photons at that height. (This can be seen by dividing the points in Figure 2 by energy to obtain the differential number flux curves).

The softening of the natural emitter  $\gamma$ -ray energy spectrum with detector height has been experimentally verified qualitatively in the field both by Gustafson *et al.*<sup>(7)</sup> and by ourselves in similar field experiments carried out in 1965 using NaI(Tl) detectors.

#### D. Differential Angular Exposure Rates

The differential angular exposure rates at the detector for three different source energies at  $h = 1$  meter, 100 meters, and 300 meters are shown in Figure 5. These curves are given in terms of exposure rate per radian due to photons traveling in the direction  $\theta$ , normalized to a total exposure rate of 1.0, where  $\theta$  is the angle relative to the

perpendicular, i.e.  $0^\circ$  is on the perpendicular to the interface heading away from the soil half space. We see from the figure that these distributions peak at around  $70^\circ - 80^\circ$  for  $h = 1$  meter,  $40^\circ - 60^\circ$  for  $h = 100$  meters, and  $30^\circ - 40^\circ$  for  $h = 300$  meters. The height of the peak decreases as the source energy decreases while the "skyshine" (photons traveling toward the ground) increases (see Table 4). As the detector height increases, the "skyshine" for a given source energy also increases. The flattening out of the angular distribution as the source energy decreases becomes more pronounced as the detector height is increased. The angular distributions of the scattered and unscattered  $\gamma$ -rays are quite comparable (see Figure 6) to the total exposure angular distributions although the unscattered distributions are slightly more peaked.

The angular exposure rate distributions for  $^{40}\text{K}$ ,  $^{238}\text{U}$ , and  $^{232}\text{Th}$  (Figure 7) are similar to those for :364, 1.0, and 2.5 MeV sources shown in Figure 5. There is little difference in the three distributions for  $h = 1$  meter and only slightly more for  $h = 100$  meters. Skyshine contributes 11% of the  $^{40}\text{K}$  exposure rate, 13% of the  $^{238}\text{U}$  exposure rate, and 12% of the  $^{232}\text{Th}$  exposure rate at  $h = 1$  meter and 12%, 15%, and 13% of the exposure rate at  $h = 100$  meters.

The natural exposure rate angular distribution, therefore, is fairly insensitive to the relative amounts of  $^{40}\text{K}$ ,  $^{238}\text{U}$ , and  $^{232}\text{Th}$  in the soil although it does vary with detector height. Thus, a detector with an angular response must be calibrated properly with elevation in order to interpret readings of natural gamma exposure rates made at various heights above the interface.

#### IV. RADIATION IN AIR DUE TO EXPONENTIALLY DISTRIBUTED (FALLOUT) SOURCES IN THE SOIL

Radioisotopes in the soil as a result of fallout from weapons tests (or accidental escape from reactors) usually remain on or just below the surface of the ground. For very short times after deposition, the sources can even be assumed to be distributed as an infinitesimally thin plane source directly on the interface. For longer lived fallout which has been in the biosphere for some time, we have found that a reasonable approximation is to assume the sources to be distributed exponentially with depth in the soil according to the relation  $S = S_0 e^{-\alpha z}$  where  $S$  is the activity at depth  $z$ ,  $S_0$  is the surface activity, and  $\alpha$  is the reciprocal of the relaxation length ( $\alpha \rightarrow \infty$  is equivalent to a plane source on the interface). For fallout deposited in the U. S. during 1962 - 1965 an assumed relaxation length of 3 cm gave a reasonable fit to actual depth distribution measurements<sup>(a)</sup>.

Many investigators calculate the exposure rate from fallout isotopes as if the source were a plane source buried at some depth  $z$  beneath the surface in order to account for the effect of ground "roughness". For a widely distributed source, for detector heights at least a meter above the interface and for a moderately flat surface, the assumption of an average exponential depth distribution should be more realistic and should also account for ground roughness since an exponential source is equivalent to burying plane sources successively deeper in the ground with decreasing intensities. The choice of the best relaxation length to use for a given source depends on such factors as the type of surface, the source energy, the time since deposition, and the type of soil.

Variations in the source energy, relaxation length, and detector height affect the exposure rate, energy spectra, and angular distributions in air. It is important to

understand the significance of these variations to properly interpret as well as predict the results of fallout measurements made either at ground level or from an airplane or helicopter. Thus, the results of our computations of radiation due to exponentially distributed sources are discussed in this light.

#### A. Exposure Rates

Total exposure rates for exponentially distributed sources of source strength one gamma emitted per  $\text{cm}^2$  of interface surface are listed in Table 5, A. Unscattered exposure rates are tabulated separately in Table 5, B. The data in Table 5 should be sufficient to allow the reader to construct exposure rate vs. height curves for any source energy and relaxation length. The dependence of the exposure rate on detector height is shown in Figures 8, 9, and 10 for several source energies and depth distributions. ( $a \rightarrow \infty$  corresponds to a plane source. All our calculations of the scattered component for a plane source were arrived at using  $a = 10,000$ . The unscattered component was calculated exactly.)

From Figures 8 and 9 we see that the variation with detector height is relatively insensitive to source energy, especially below  $h = 100$  meters. Figure 10 illustrates the effect of the depth distribution on the exposure rate at various detector heights. The scattered component falls off very slowly with height all the way up to about  $h = 30$  meters, but as the depth distribution approaches a plane source the unscattered component causes the total exposure rate to begin to drop off more quickly with height. The exposure rates for various depth distributions all tend to converge at higher altitudes, i.e. the effect of the source depth distribution is reduced. This is qualitatively what we would expect when using an exponential source distribution model to represent ground roughness, since ground roughness effects decrease as the detector height is increased.

From Figure 11 we see that the ratio of the exposure rates at  $h = 1$  meter even for two sources quite far apart in energy does not depend on the depth distribution. This is important since often one can make the assumption that two isotopes are distributed similarly with depth. If one then has an experimental measure of the ratio of their activities at any depth one can, using the results of this report, estimate the ratios of their exposure rates. If an independent measure of the total exposure rate can then be made, a fairly complete picture of the radiation field can be deduced.

A more detailed examination of the variation in exposure rate with detector height is shown in Figure 12 where the ratios of the exposure rates at 10, 100, and 300 meters to that at 1 meter are plotted for different source distributions. Here we see that the 10 meter/1 meter and 100 meter/1 meter ratios do not vary too rapidly with source energy. Since over a wide range of depth distributions this ratio changes by only a factor of about 2, one can make reasonable estimates of the exposure rate at ground level using measurements made from an airplane or helicopter even if the exact source spectrum of the radiation is unknown. This fact could be of importance for some types of emergency radiological surveying procedures.

Figure 13 indicates the ratio of the exposure rate due to scattered  $\gamma$ -rays relative to the total exposure. The shape of the curves for  $h = 1$  meter and  $h = 100$  meters is fairly similar, reflecting corresponding dependence on source energy. The percentage of the scattered component to the total, as determined from Figure 10, however, is much more dependent on the source depth distribution at  $h = 1$  meter than it is at  $h = 100$  meters. This again indicates the increased effect of the extra soil cover on exposure rates at lower detector heights relative to higher altitudes.

The fractions of the total exposure rate due to "skyshine" are given in Table 6. The "skyshine" is quite

sensitive to both source energy and detector height and becomes a very significant portion of the total exposure rate at low source energies and higher detector positions.

#### B. Differential Energy Spectra

The effect of the source depth distribution on the differential energy spectra of the scattered energy flux is shown in Figure 14 for a .662 MeV ( $^{137}\text{Cs}$ ) source. At  $h = 1$  meter the spectrum for the distributed source ( $\alpha = .33$ ) is softer than that for the plane source while at  $h = 100$  meters there is little difference in the shapes of the two spectra. Thus, it would not be possible to make inferences about the depth distribution or the exact exposure rate at ground level by using an altitude measurement of the energy spectra.

#### C. Integral Exposure Spectra

The softening of the scattered energy flux spectra at  $h = 1$  meter results in a corresponding softening in the integral exposure rate spectra (Figures 15, 16, 17) especially for  $h = 1$  meter. All three figures show the same general features. The diminished influence of the source depth distribution at  $h = 100$  meters is evident. The fraction of the exposure rate due to  $\gamma$ -rays below a given energy,  $E$ , increases and the total scattered component increases as the source energy decreases, comparable to the result we obtained for the uniformly distributed sources. Again, we must emphasize the need to properly interpret energy dependent dosimeter readings, since at  $h = 100$  meters over 20% of the exposure rate from an  $^{131}\text{I}$  source (.364 MeV) is due to  $\gamma$ -rays of energy less than 100 keV as opposed to a corresponding 6% for 1.25 MeV ( $^{60}\text{Co}$ )  $\gamma$ -rays.

#### D. Angular Distributions

For a plane source or even a source distributed slightly with depth, at detector heights close to the interface the

largest portion of the exposure rate is due to unscattered  $\gamma$ -rays (Figure 13). The direct beam or unscattered  $\gamma$ -ray angular distributions at such source depths rise to a very sharp peak in the angular region  $\theta = 89^\circ - 90^\circ$ , and this peak dominates the scattered component and results in a very skewed total exposure rate angular distribution (Figure 18a). The shape of this distribution is slightly dependent on source energy becoming less peaked as the source energy decreases. The sharpness of the peak is only slightly diminished as the source becomes more deeply distributed in the ground and is still very acute even for  $\alpha = .33$ . The angular distributions flatten out considerably as the detector height is increased but even at  $h = 100$  meters (Figures 18a and 18b) these are still more peaked than the corresponding distributions for uniformly distributed sources (Figures 5 and 6). The peaks of the curves for  $\alpha = .33$  (Figure 18b) are slightly reduced and shifted toward the vertical ( $\theta = 0^\circ$ ) compared to the corresponding curves for the plane source. This fact might be useful in estimating the depth distribution of a given isotope from an angular distribution measurement taken in an airplane or helicopter.

Since the response of almost all instruments has some angular dependence, our observations are significant for interpreting field measurements. It is clear from the data presented here that careful instrument calibrations are essential in order to properly interpret measurements made at different detector heights.

## V. CONCLUSIONS

The energy spectra and angular exposure rate distributions for fallout sources differ considerably from those for the natural emitters because of the different source depth distributions. The magnitude of this difference depends on the exact depth distribution of the fallout emitters. The computations in this report indicate that both distributions also vary with detector height, emphasizing the necessity of carefully calibrating detectors used for measuring gamma radiation in the field.

The calculated exposure rates, differential energy spectra, and angular exposure rates can be used for interpreting and analyzing the results of land and aerial surveys over extensively contaminated areas as well as for predicting the results of such surveys for a known level of contamination. In certain instances experimental data taken at high altitudes can be used to infer information about the radiation field near the interface. This can be done by utilizing the curves given in this report, taking into account the source spectrum and depth distribution of the isotopes contributing to the field.

## REFERENCES

1. Beck, H. L., Condon, W. J., and Lowder, W. M.  
Spectrometric Techniques for Measuring Environmental  
Gamma Radiation  
USAEC Report HASL-150, October (1964)
2. Bennett, B. G. and Beck, H. L.  
Legendre, Tschebyscheff, and Half-Range Legendre Polynomial  
Solutions of the Gamma Ray Transport Equation in Infinite  
Homogeneous and Two Media Plane Geometry  
USAEC Report HASL-185, August (1967)
3. Lanning, W. D.  
Application of the Spherical Harmonics Technique to  
Problems in Gamma Transport  
Nucl. Sci. and Eng., 15, 259-267 (1963)
4. Hubbell, J. H. and Berger, M. J.  
Photon Attenuation and Energy Transfer Coefficients,  
Tabulations and Discussions  
NBS Report 8681, May (1965)
5. Gerasimov, I. P. and Glazovskaya, M. A.  
Fundamentals of Soil Science and Soil Geography,  
Gosudarstvennoe Izdatel'stvo Geograficheskoi Liter-  
atury, Moskva 1960  
Translated from Russian by Israel Program for Scientific  
Translations, Jerusalem (1965)
6. Beck, H. L., Lowder, W. M., Bennett, B. G., and  
Condon, W. J.  
Further Studies of External Environmental Radiation  
USAEC Report HASL-170, March (1966)

7. Gustafson, F., Kastner, J., and Luetzelschwab, J.  
Environmental Radiation Measurement of Dose Rates  
Science, 145, 44-47 (1964)
8. Beck, Harold L.  
Environmental Gamma Radiation from Deposited Fission  
Products, 1960-1964  
Health Physics, 12, 313-322 (1966)

TABLE 1  
SOURCE SPECTRA USED FOR  $^{238}\text{U}$  and  $^{232}\text{Th}$  EXPOSURE  
RATE CALCULATIONS

$^{238}\text{U}$ Series		$^{232}\text{Th}$ Series	
Source Energy (MeV)	Photons per Disintegration	Source Energy (MeV)	Photons per Disintegration
.24	.11	.16	.12
.29	.24	.24	.80
.35	.38	.33	.19
.49	.08	.44	.05
.61	.42	.51	.09
.77	.11	.58	.30
.94	.04	.73	.10
1.12	.19	.92	.56
1.24	.08	1.60	.28
1.39	.09	1.80	.01
1.58	.06	2.62	.35
1.76	.21		
2.20	.08		
2.44	.02		

TABLE 2  
EXPOSURE RATES - UNIFORMLY DISTRIBUTED SOURCE\*

		A. Total Exposure Rate†									
E (MeV)	h (m)	0	.1	.5	1	3	5	10	30	100	300
.25	6.24 (-2)	6.23 (-2)	6.16 (-2)	5.99 (-2)	5.88 (-2)	5.71 (-2)	5.33 (-2)	4.24 (-2)	2.04 (-2)	2.42 (-2)	
.364	9.92 (-2)	9.89 (-2)	9.79 (-2)	9.68 (-2)	9.34 (-2)	9.06 (-2)	8.48 (-2)	6.74 (-2)	3.38 (-2)	4.75 (-3)	
.50	1.40 (-1)	1.38 (-1)	1.37 (-1)	1.32 (-1)	1.28 (-1)	1.20 (-1)	9.62 (-2)	4.95 (-2)	8.06 (-3)		
.662	1.91 (-1)	1.90 (-1)	1.88 (-1)	1.86 (-1)	1.80 (-1)	1.75 (-1)	1.64 (-1)	1.32 (-1)	7.02 (-2)	1.32 (-2)	
.75	2.19 (-1)	2.19 (-1)	2.17 (-1)	2.14 (-1)	2.07 (-1)	2.01 (-1)	1.89 (-1)	1.53 (-1)	8.26 (-2)	1.63 (-2)	
1.0	2.95 (-1)	2.94 (-1)	2.91 (-1)	2.88 (-1)	2.79 (-1)	2.71 (-1)	2.55 (-1)	2.07 (-1)	1.16 (-1)	2.62 (-2)	
1.25	3.72 (-1)	3.71 (-1)	3.68 (-1)	3.64 (-1)	3.53 (-1)	3.43 (-1)	3.25 (-1)	2.66 (-1)	1.53 (-1)	3.86 (-2)	
1.46	4.36 (-1)	4.35 (-1)	4.32 (-1)	4.28 (-1)	4.15 (-1)	4.04 (-1)	3.83 (-1)	3.16 (-1)	1.85 (-1)	4.99 (-2)	
1.76	5.26 (-1)	5.25 (-1)	5.21 (-1)	5.18 (-1)	5.02 (-1)	4.89 (-1)	4.64 (-1)	3.86 (-1)	2.34 (-1)	6.83 (-2)	
2.00	6.01 (-1)	6.00 (-1)	5.95 (-1)	5.90 (-1)	5.73 (-1)	5.60 (-1)	5.31 (-1)	4.45 (-1)	2.75 (-1)	8.38 (-2)	
2.25	6.70 (-1)	6.69 (-1)	6.64 (-1)	6.59 (-1)	6.40 (-1)	6.26 (-1)	5.95 (-1)	5.01 (-1)	3.14 (-1)	1.01 (-1)	
2.50	7.44 (-1)	7.43 (-1)	7.37 (-1)	7.32 (-1)	7.12 (-1)	6.96 (-1)	6.62 (-1)	5.61 (-1)	3.55 (-1)	1.20 (-1)	
2.62	7.83 (-1)	7.81 (-1)	7.75 (-1)	7.69 (-1)	7.49 (-1)	7.32 (-1)	6.97 (-1)	5.93 (-1)	3.79 (-1)	1.30 (-1)	
2.75	8.19 (-1)	8.18 (-1)	8.12 (-1)	8.06 (-1)	7.85 (-1)	7.67 (-1)	7.32 (-1)	6.22 (-1)	4.01 (-1)	1.40 (-1)	

\*Source Strength = 1  $\gamma$  per  $\text{cm}^3\text{-sec}$ .

†MeV/gm-sec = 65.9  $\mu\text{r}/\text{hr}$ ; 1  $\mu\text{r}/\text{hr}$  = 7.65 mrad/yr.

TABLE 2 (Cont'd)

B. Unscattered  $\gamma$ -Rays†

$E$ (MeV) \ $h$ (m)	0	.1	.5	1	3	5	10	30	100	300
.25	1.89 (-2)	1.87 (-2)	1.77 (-2)	1.60 (-2)	1.48 (-2)	1.25 (-2)	7.21 (-3)	1.65 (-3)	5.31 (-5)	
.364	3.33 (-2)	3.31 (-2)	3.22 (-2)	3.14 (-2)	2.88 (-2)	2.68 (-2)	2.29 (-2)	1.40 (-2)	3.70 (-3)	1.72 (-4)
.50	5.32 (-2)	5.28 (-2)	5.16 (-2)	5.04 (-2)	4.66 (-2)	4.37 (-2)	3.79 (-2)	2.42 (-2)	7.34 (-3)	4.71 (-4)
.662	7.87 (-2)	7.83 (-2)	7.67 (-2)	7.50 (-2)	6.99 (-2)	6.59 (-2)	5.80 (-2)	3.85 (-2)	1.30 (-2)	1.09 (-3)
.75	9.36 (-2)	9.31 (-2)	9.13 (-2)	8.94 (-2)	8.35 (-2)	7.90 (-2)	6.98 (-2)	4.72 (-2)	1.67 (-2)	1.58 (-3)
1.0	1.37 (-1)	1.36 (-1)	1.34 (-1)	1.31 (-1)	1.24 (-1)	1.17 (-1)	1.05 (-1)	7.38 (-2)	2.90 (-2)	3.51 (-3)
1.25	1.82 (-1)	1.81 (-1)	1.79 (-1)	1.76 (-1)	1.66 (-1)	1.58 (-1)	1.43 (-1)	1.04 (-1)	4.41 (-2)	6.46 (-3)
1.46	2.22 (-1)	2.21 (-1)	2.18 (-1)	2.15 (-1)	2.03 (-1)	1.95 (-1)	1.77 (-1)	1.31 (-1)	5.84 (-2)	9.63 (-3)
1.76	2.80 (-1)	2.79 (-1)	2.75 (-1)	2.71 (-1)	2.58 (-1)	2.48 (-1)	2.27 (-1)	1.71 (-1)	8.10 (-2)	1.53 (-2)
2.00	3.27 (-1)	3.26 (-1)	3.22 (-1)	3.17 (-1)	3.02 (-1)	2.91 (-1)	2.68 (-1)	2.04 (-1)	1.01 (-1)	2.07 (-2)
2.25	3.73 (-1)	3.72 (-1)	3.67 (-1)	3.62 (-1)	3.47 (-1)	3.34 (-1)	3.09 (-1)	2.39 (-1)	1.21 (-1)	2.70 (-2)
2.50	4.23 (-1)	4.22 (-1)	4.17 (-1)	4.12 (-1)	3.95 (-1)	3.81 (-1)	3.53 (-1)	2.75 (-1)	1.44 (-1)	3.39 (-2)
2.62	4.50 (-1)	4.49 (-1)	4.44 (-1)	4.39 (-1)	4.21 (-1)	4.06 (-1)	3.77 (-1)	2.97 (-1)	1.58 (-1)	3.91 (-2)
2.75	4.74 (-1)	4.73 (-1)	4.68 (-1)	4.62 (-1)	4.44 (-1)	4.29 (-1)	3.98 (-1)	3.14 (-1)	1.68 (-1)	4.21 (-2)

† MeV/gram-sec = 65.9  $\mu$ r/hr; 1  $\mu$ r/hr = 7.65 mrad/yr.

TABLE 3

EXPOSURE RATES IN AIR DUE TO  $^{40}\text{K}$ ,  $^{238}\text{U}$ , and  $^{232}\text{Th}$  IN THE SOIL ( $\mu\text{r}/\text{hr}$ )

Detector Height (meters)	Exposure Rate* per 1% $^{40}\text{K}$	% Decrease from 0 Meter Value	Exposure Rate* per 1 ppm $^{238}\text{U}$ #	% Decrease from 0 Meter Value	Exposure Rate* per 1 ppm $^{232}\text{Th}$	% Decrease from 0 Meter Value
0	1.68	0	.667	0	.314	0
1	1.65	2	.654	2	.307	2
	(1.71†)		(.76†)		(.36†)	
3	1.60	5	.635	5	.298	5
5	1.56	7	.618	7	.290	8
10	1.47	13	.583	13	.274	13
30	1.22	27	.476	29	.226	28
100	0.72	57	.274	59	.133	58
300	0.19	89	.068	90	.036	89

\* $1\% \text{ }^{40}\text{K} = .0586 \text{ dis/cm}^3$ ,  $1 \text{ ppm } ^{238}\text{U} = .0198 \text{ dis/cm}^3$ ,  $1 \text{ ppm } ^{232}\text{Th} = 6.57 \times 10^{-3}$  dis/cm<sup>3</sup>, soil density,  $\rho = 1.6 \text{ gm/cm}^3$ .

†Previously reported values (1).

#Exposure rate due to radon daughters in the atmosphere has been neglected but should not amount to more than a few percent of the total exposure rate even close to the interface (1,6).

TABLE 4

PERCENTAGE OF TOTAL EXPOSURE RATE DUE TO SKYSHINE FOR  
UNIFORMLY DISTRIBUTED SOURCES

<u>Source</u>	<u><math>h = 1</math> meter</u>	<u><math>h = 100</math> meters</u>
.364 MeV	21%	24%
1.0 MeV	13%	16%
2.5 MeV	8.6%	9.5%
$^{238}_{\alpha}$ U series	13%	15%
$^{40}_{\alpha}$ K	11%	12%
$^{232}_{\alpha}$ Th series	12%	13%

TABLE 5  
EXPOSURE RATES - EXPONENTIALLY DISTRIBUTED SOURCE\*

		A. Total Exposure Rate†								
		$\alpha^{\ddagger} = .1$								
E (MeV)	h (m)	0	.1	1	3	5	10	30	100	300
.25	4.06 (-3)	3.91 (-3)	3.68 (-3)	3.53 (-3)	3.32 (-3)	2.23 (-3)	8.63 (-4)	1.20 (-4)		
.364	6.34 (-3)	6.31 (-3)	6.13 (-3)	5.86 (-3)	5.65 (-3)	5.20 (-3)	3.99 (-3)	1.89 (-3)	2.84 (-4)	
.50	8.73 (-3)	8.70 (-3)	8.47 (-3)	8.07 (-3)	7.78 (-3)	7.18 (-3)	6.33 (-3)	2.70 (-3)	4.52 (-4)	
.662	1.16 (-2)	1.15 (-2)	1.12 (-2)	1.07 (-2)	1.03 (-2)	9.50 (-3)	7.38 (-3)	3.72 (-3)	7.04 (-4)	
.75	1.31 (-2)	1.31 (-2)	1.27 (-2)	1.21 (-2)	1.17 (-2)	1.08 (-2)	8.37 (-3)	4.25 (-3)	8.53 (-4)	
1.0	1.72 (-2)	1.71 (-2)	1.67 (-2)	1.59 (-2)	1.54 (-2)	1.42 (-2)	1.11 (-2)	5.87 (-3)	1.33 (-3)	
1.25	2.11 (-2)	2.09 (-2)	2.02 (-2)	1.96 (-2)	1.89 (-2)	1.76 (-2)	1.39 (-2)	7.43 (-3)	1.86 (-3)	

\*Source strength = 1  $\gamma$  per  $\text{cm}^2\text{-sec}$ .

† $\text{Mray/gm-sec} = 65.9 \mu\text{r/hr}; 1 \mu\text{r/hr} = 7.65 \text{ mrad/yr}$ .

‡ $\alpha$  is the reciprocal of the relaxation length which defines the depth distribution (see page 14).

TABLE 5 (Cont'd)

$E$	$h$	0	.1	1	3	5	10	30	100	300
$\alpha = .33$										
.25	7.82 (-3)	7.55 (-3)	7.45 (-3)	6.93 (-3)	6.55 (-3)	6.03 (-3)	3.90 (-3)	1.44 (-3)	1.98 (-4)	
.364	1.24 (-2)	1.22 (-2)	1.17 (-2)	1.11 (-2)	1.09 (-2)	9.47 (-3)	7.10 (-3)	3.18 (-3)	4.80 (-4)	
.50	1.67 (-2)	1.66 (-2)	1.56 (-2)	1.50 (-2)	1.42 (-2)	1.29 (-2)	9.64 (-3)	4.48 (-3)	7.43 (-4)	
.662	2.172 (-2)	2.16 (-2)	2.08 (-2)	1.95 (-2)	1.864 (-2)	1.69 (-2)	1.257 (-2)	6.02 (-3)	1.12 (-3)	
.75	2.455 (-2)	2.435 (-2)	2.34 (-2)	2.20 (-2)	2.10 (-2)	1.90 (-2)	1.412 (-2)	6.82 (-3)	1.34 (-3)	
1.0	3.17 (-2)	3.15 (-2)	3.03 (-2)	2.85 (-2)	2.72 (-2)	2.46 (-2)	1.85 (-2)	9.19 (-3)	2.03 (-3)	
1.25	3.87 (-2)	3.81 (-2)	3.66 (-2)	3.46 (-2)	3.29 (-2)	3.00 (-2)	2.27 (-2)	1.15 (-2)	2.86 (-3)	
2.25	6.11 (-2)	6.08 (-2)	6.06 (-2)	5.52 (-2)	5.27 (-2)	4.83 (-2)	3.75 (-2)	2.01 (-2)	5.77 (-3)	
$\alpha = .5$										
.25	9.34 (-3)	9.02 (-3)	8.84 (-3)	8.16 (-3)	7.69 (-3)	7.03 (-3)	4.48 (-3)	1.61 (-3)	2.23 (-4)	
.364	1.44 (-2)	1.43 (-2)	1.36 (-2)	1.27 (-2)	1.21 (-2)	1.09 (-2)	7.91 (-3)	3.52 (-3)	5.30 (-4)	
.50	1.96 (-2)	1.94 (-2)	1.86 (-2)	1.73 (-2)	1.64 (-2)	1.47 (-2)	1.08 (-2)	4.95 (-3)	8.20 (-4)	
.662	2.55 (-2)	2.54 (-2)	2.42 (-2)	2.26 (-2)	2.15 (-2)	1.92 (-2)	1.41 (-2)	6.60 (-3)	1.24 (-3)	
.75	2.87 (-2)	2.85 (-2)	2.73 (-2)	2.54 (-2)	2.41 (-2)	2.16 (-2)	1.58 (-2)	7.47 (-3)	1.46 (-3)	
1.0	3.72 (-2)	3.68 (-2)	3.52 (-2)	3.28 (-2)	3.12 (-2)	2.80 (-2)	2.06 (-2)	1.01 (-2)	2.19 (-3)	
1.25	4.48 (-2)	4.45 (-2)	4.23 (-2)	3.96 (-2)	3.76 (-2)	3.40 (-2)	2.52 (-2)	1.25 (-2)	3.02 (-3)	

TABLE 5 (Cont'd)

TABLE 5 (Cont'd)

		Plane Source							
E (MeV) \ h (m)	0	.1	1	3	5	10	30	100	300
.25	2.67(-2)	1.89(-2)	1.500(-2)	1.33(-2)	1.12(-2)	6.42(-3)	2.09(-3)	2.87(-4)	
.364	4.11(-2)	2.89(-2)	2.31(-2)	2.05(-2)	1.68(-2)	1.02(-2)	4.50(-3)	6.79(-4)	
.50	5.65(-2)	3.95(-2)	3.12(-2)	2.77(-2)	2.28(-2)	1.50(-2)	6.31(-3)	1.02(-3)	
.662	6.36(-2)	5.14(-2)	4.05(-2)	3.59(-2)	2.96(-2)	1.934(-2)	8.37(-3)	1.51(-3)	
.75	7.19(-2)	5.77(-2)	4.55(-2)	4.03(-2)	3.32(-2)	2.16(-2)	9.37(-3)	1.79(-3)	
1.0	1.057(-1)	7.38(-2)	5.94(-2)	5.14(-2)	4.26(-2)	2.79(-2)	1.24(-2)	2.61(-3)	
1.17	1.19(-1)	8.37(-2)	6.64(-2)	5.82(-2)	4.83(-2)	3.18(-2)	1.44(-2)	3.17(-3)	
1.25	1.27(-1)	8.89(-2)	7.06(-2)	6.18(-2)	5.13(-2)	3.39(-2)	1.55(-2)	3.50(-3)	
1.33	1.33(-1)	9.34(-2)	7.43(-2)	6.50(-2)	5.40(-2)	3.57(-2)	1.66(-2)	3.92(-3)	
1.76	1.65(-1)	1.18(-1)	9.33(-2)	8.13(-2)	6.76(-2)	4.52(-2)	2.08(-2)	5.48(-3)	
2.25	1.97(-1)	1.38(-1)	1.12(-1)	9.65(-2)	7.96(-2)	5.22(-2)	2.58(-2)	6.95(-3)	
2.75	2.29(-1)	1.59(-1)	1.33(-1)	1.15(-1)	9.61(-2)	6.52(-2)	3.09(-2)	9.69(-3)	

TABLE 5 (Cont'd)

B. Unscattered  $\gamma$ -rays\*

$E$ (MeV)	$h$ (m)	0	.1	1	3	5	10	30	100	300
$\alpha = .1$										
.25	1.51 (-3)	1.49 (-3)	1.39 (-3)	1.25 (-3)	1.15 (-3)	9.54 (-4)	5.34 (-4)	1.17 (-4)	3.61 (-6)	
.364	2.59 (-3)	2.57 (-3)	2.41 (-3)	2.19 (-3)	2.02 (-3)	1.70 (-3)	1.00 (-3)	2.53 (-4)	1.12 (-5)	
.50	4.02 (-3)	3.99 (-3)	3.77 (-3)	3.44 (-3)	3.20 (-3)	2.74 (-3)	1.69 (-3)	4.84 (-4)	2.95 (-5)	
.662	5.77 (-3)	5.73 (-3)	5.44 (-3)	5.01 (-3)	4.68 (-3)	4.05 (-3)	2.59 (-3)	8.26 (-4)	6.57 (-5)	
.75	6.76 (-3)	6.72 (-3)	6.39 (-3)	5.89 (-3)	5.53 (-3)	4.81 (-3)	3.13 (-3)	1.04 (-3)	9.23 (-5)	
1.0	9.53 (-3)	9.48 (-3)	9.05 (-3)	8.40 (-3)	7.91 (-3)	6.96 (-3)	4.69 (-3)	1.73 (-3)	1.96 (-4)	
1.25	1.23 (-2)	1.22 (-2)	1.17 (-2)	1.09 (-2)	1.03 (-2)	9.18 (-3)	6.36 (-3)	2.53 (-3)	3.46 (-4)	
$\alpha = .33$										
.25	3.59 (-3)	3.54 (-3)	3.26 (-3)	2.89 (-3)	2.61 (-3)	2.12 (-3)	1.13 (-3)	2.35 (-4)	6.93 (-6)	
.364	5.99 (-3)	5.93 (-3)	5.49 (-3)	4.89 (-3)	4.46 (-3)	3.67 (-3)	2.06 (-3)	4.90 (-4)	2.07 (-5)	
.50	9.08 (-3)	8.99 (-3)	8.36 (-3)	7.51 (-3)	6.89 (-3)	5.76 (-3)	3.38 (-3)	9.11 (-4)	5.29 (-5)	
.662	1.27 (-2)	1.26 (-2)	1.18 (-2)	1.07 (-2)	9.83 (-3)	8.31 (-3)	5.06 (-3)	1.51 (-3)	1.14 (-4)	
.75	1.48 (-2)	1.46 (-2)	1.37 (-2)	1.24 (-2)	1.15 (-2)	9.75 (-3)	6.03 (-3)	1.89 (-3)	1.59 (-4)	
1.0	2.02 (-2)	2.01 (-2)	1.89 (-2)	1.72 (-2)	1.60 (-2)	1.37 (-2)	8.80 (-3)	3.03 (-3)	3.25 (-4)	
1.25	2.55 (-2)	2.54 (-2)	2.40 (-2)	2.19 (-2)	2.04 (-2)	1.77 (-2)	1.17 (-2)	4.33 (-3)	5.59 (-4)	
1.76	3.60 (-2)	3.58 (-2)	3.40 (-2)	3.12 (-2)	2.93 (-2)	2.57 (-2)	1.76 (-2)	7.20 (-3)	1.19 (-3)	
2.25	4.50 (-2)	4.47 (-2)	4.26 (-2)	3.93 (-2)	3.70 (-2)	3.28 (-2)	2.29 (-2)	1.01 (-2)	1.94 (-3)	
2.75	5.39 (-2)	5.36 (-2)	5.12 (-2)	4.74 (-2)	4.47 (-2)	3.98 (-2)	2.84 (-2)	1.30 (-2)	2.81 (-3)	

\* MeV/gm-sec = 65.9  $\mu$ r/hr; 1  $\mu$ r/hr = 7.65 mrad/yr.

TABLE 5 (Cont'd)

$E$ (MeV)	$n$ (m)	0	.1	1	3	5	10	30	100	300
$\alpha = .50$										
.25	4.56 (-3)	4.50 (-3)	4.11 (-3)	3.60 (-3)	3.24 (-3)	2.60 (-3)	1.36 (-3)	2.74 (-4)	7.98 (-6)	
.364	7.55 (-3)	7.45 (-3)	6.84 (-3)	6.03 (-3)	5.47 (-3)	4.45 (-3)	2.45 (-3)	5.67 (-4)	2.36 (-5)	
.50	1.13 (-2)	1.12 (-2)	1.03 (-2)	9.19 (-3)	8.39 (-3)	6.93 (-3)	3.98 (-3)	1.05 (-3)	5.97 (-5)	
.662	1.58 (-2)	1.56 (-2)	1.45 (-2)	1.29 (-2)	1.19 (-2)	9.92 (-3)	5.91 (-3)	1.72 (-3)	1.28 (-4)	
.75	1.82 (-2)	1.80 (-2)	1.68 (-2)	1.50 (-2)	1.38 (-2)	1.16 (-2)	7.02 (-3)	2.14 (-3)	1.77 (-4)	
1.0	2.48 (-2)	2.45 (-2)	2.29 (-2)	2.06 (-2)	1.91 (-2)	1.62 (-2)	1.02 (-2)	3.41 (-3)	3.59 (-4)	
1.25	3.11 (-2)	3.08 (-2)	2.89 (-2)	2.61 (-2)	2.42 (-2)	2.08 (-2)	1.34 (-2)	4.85 (-3)	6.14 (-4)	
1.76	4.33 (-2)	4.30 (-2)	4.05 (-2)	3.69 (-2)	3.44 (-2)	2.99 (-2)	2.00 (-2)	7.98 (-3)	1.29 (-3)	
2.25	5.38 (-2)	5.34 (-2)	5.05 (-2)	4.61 (-2)	4.32 (-2)	3.78 (-2)	2.59 (-2)	1.11 (-2)	2.09 (-3)	
2.75	6.41 (-2)	6.37 (-2)	6.04 (-2)	5.54 (-2)	5.19 (-2)	4.57 (-2)	3.19 (-2)	1.43 (-2)	3.02 (-3)	
$\alpha = 1.0$										
.25	6.47 (-3)	6.36 (-3)	5.69 (-3)	4.88 (-3)	4.33 (-3)	3.40 (-3)	1.71 (-3)	3.32 (-4)	9.42 (-6)	
.364	1.05 (-2)	1.04 (-2)	9.33 (-3)	8.06 (-3)	7.21 (-3)	5.74 (-3)	3.03 (-3)	6.76 (-4)	2.74 (-5)	
.50	1.57 (-2)	1.54 (-2)	1.40 (-2)	1.21 (-2)	1.09 (-2)	8.84 (-3)	4.88 (-3)	1.23 (-3)	6.86 (-5)	
.662	2.15 (-2)	2.12 (-2)	1.93 (-2)	1.69 (-2)	1.53 (-2)	1.25 (-2)	7.16 (-3)	2.01 (-3)	1.45 (-4)	
.75	2.47 (-2)	2.44 (-2)	2.22 (-2)	1.95 (-2)	1.77 (-2)	1.46 (-2)	8.46 (-3)	2.47 (-3)	2.00 (-4)	
1.0	3.32 (-2)	3.28 (-2)	3.01 (-2)	2.65 (-2)	2.42 (-2)	2.01 (-2)	1.21 (-2)	3.91 (-3)	4.02 (-4)	
1.25	4.13 (-2)	4.08 (-2)	3.76 (-2)	3.32 (-2)	3.04 (-2)	2.56 (-2)	1.58 (-2)	5.51 (-3)	6.81 (-4)	
1.76	5.68 (-2)	5.62 (-2)	5.21 (-2)	4.63 (-2)	4.26 (-2)	3.63 (-2)	2.33 (-2)	8.98 (-3)	1.41 (-3)	
2.25	6.98 (-2)	6.91 (-2)	6.43 (-2)	5.74 (-2)	5.30 (-2)	4.56 (-2)	3.01 (-2)	1.24 (-2)	2.28 (-3)	
2.75	8.25 (-2)	8.18 (-2)	7.64 (-2)	6.84 (-2)	6.32 (-2)	5.47 (-2)	3.68 (-2)	1.59 (-2)	3.27 (-3)	

TABLE 5 (Cont'd)

$E$ (MeV)	$h$ (m)	0	.1	1	3	5	10	30	100	300
<u><math>\alpha = 10.0</math></u>										
.25	1.39 (-2)	1.34 (-2)	1.05 (-2)	8.10 (-3)	6.86 (-3)	5.01 (-3)	2.28 (-3)	4.11 (-4)	1.13 (-5)	
.364	2.20 (-2)	2.13 (-2)	1.68 (-2)	1.30 (-2)	1.11 (-2)	8.28 (-3)	3.96 (-3)	8.22 (-4)	3.21 (-5)	
.50	3.19 (-2)	3.08 (-2)	2.47 (-2)	1.92 (-2)	1.66 (-2)	1.25 (-2)	6.27 (-3)	1.48 (-3)	7.93 (-5)	
.662	4.27 (-2)	4.15 (-2)	3.36 (-2)	2.62 (-2)	2.27 (-2)	1.75 (-2)	9.08 (-3)	2.37 (-3)	1.65 (-4)	
.75	4.86 (-2)	4.72 (-2)	3.84 (-2)	2.99 (-2)	2.60 (-2)	2.02 (-2)	1.07 (-2)	2.91 (-3)	2.27 (-4)	
1.0	6.36 (-2)	6.19 (-2)	5.11 (-2)	4.00 (-2)	3.48 (-2)	2.74 (-2)	1.50 (-2)	4.53 (-3)	4.50 (-4)	
1.25	7.74 (-2)	7.56 (-2)	6.30 (-2)	4.96 (-2)	4.33 (-2)	3.44 (-2)	1.95 (-2)	6.33 (-3)	7.57 (-4)	
<u>Plane Source</u>										
.25	2.09 (-2)	1.29 (-2)	9.13 (-3)	7.55 (-3)	5.37 (-3)	2.38 (-3)	4.23 (-4)	1.15 (-5)		
.364	3.27 (-2)	2.05 (-2)	1.47 (-2)	1.22 (-2)	8.88 (-3)	4.15 (-3)	8.56 (-4)	3.40 (-5)		
.50	4.69 (-2)	2.98 (-2)	2.15 (-2)	1.80 (-2)	1.33 (-2)	6.50 (-3)	1.51 (-3)	8.07 (-5)		
.662	6.25 (-2)	4.01 (-2)	2.92 (-2)	2.46 (-2)	1.85 (-2)	9.36 (-3)	2.41 (-3)	1.67 (-4)		
.75	7.07 (-2)	4.56 (-2)	3.34 (-2)	2.82 (-2)	2.13 (-2)	1.10 (-2)	2.97 (-3)	2.31 (-4)		
1.0	9.21 (-2)	6.00 (-2)	4.46 (-2)	3.76 (-2)	2.89 (-2)	1.55 (-2)	4.62 (-3)	4.57 (-4)		
1.17	1.05 (-1)	6.91 (-2)	5.17 (-2)	4.36 (-2)	3.38 (-2)	1.85 (-2)	5.79 (-3)	6.38 (-4)		
1.25	1.12 (-1)	7.38 (-2)	5.55 (-2)	4.67 (-2)	3.63 (-2)	2.01 (-2)	6.44 (-3)	7.61 (-4)		
1.33	1.18 (-1)	7.79 (-2)	5.88 (-2)	4.95 (-2)	3.86 (-2)	2.15 (-2)	7.04 (-3)	8.73 (-4)		
1.76	1.48 (-1)	9.85 (-2)	7.57 (-2)	6.37 (-2)	5.01 (-2)	2.90 (-2)	1.03 (-2)	1.57 (-3)		
2.25	1.77 (-1)	1.19 (-1)	9.30 (-2)	7.83 (-2)	6.18 (-2)	3.68 (-2)	1.40 (-2)	2.47 (-3)		
2.75	2.07 (-1)	1.39 (-1)	1.11 (-1)	9.32 (-2)	7.38 (-2)	4.51 (-2)	1.81 (-2)	3.61 (-3)		

TABLE 6

PERCENTAGE OF TOTAL EXPOSURE RATE DUE TO SKYSHINE-  
EXPONENTIALLY DISTRIBUTED SOURCES

Source	$h = 1$ meter	$h = 100$ meters
$\alpha = .33 \left\{ \begin{array}{l} .364 \text{ MeV} \\ .662 \text{ MeV} \\ 1.25 \text{ MeV} \end{array} \right.$	17.6%	23.1%
	13.9%	18.6%
	10.1%	13.3%
Plane* $\left\{ \begin{array}{l} .364 \text{ MeV} \\ .662 \text{ MeV} \\ 1.25 \text{ MeV} \end{array} \right.$	11.8%	23.1%
	9.5%	18.0%
	8.0%	12.9%

\* $\alpha \rightarrow \infty$  corresponds to an infinite plane source.

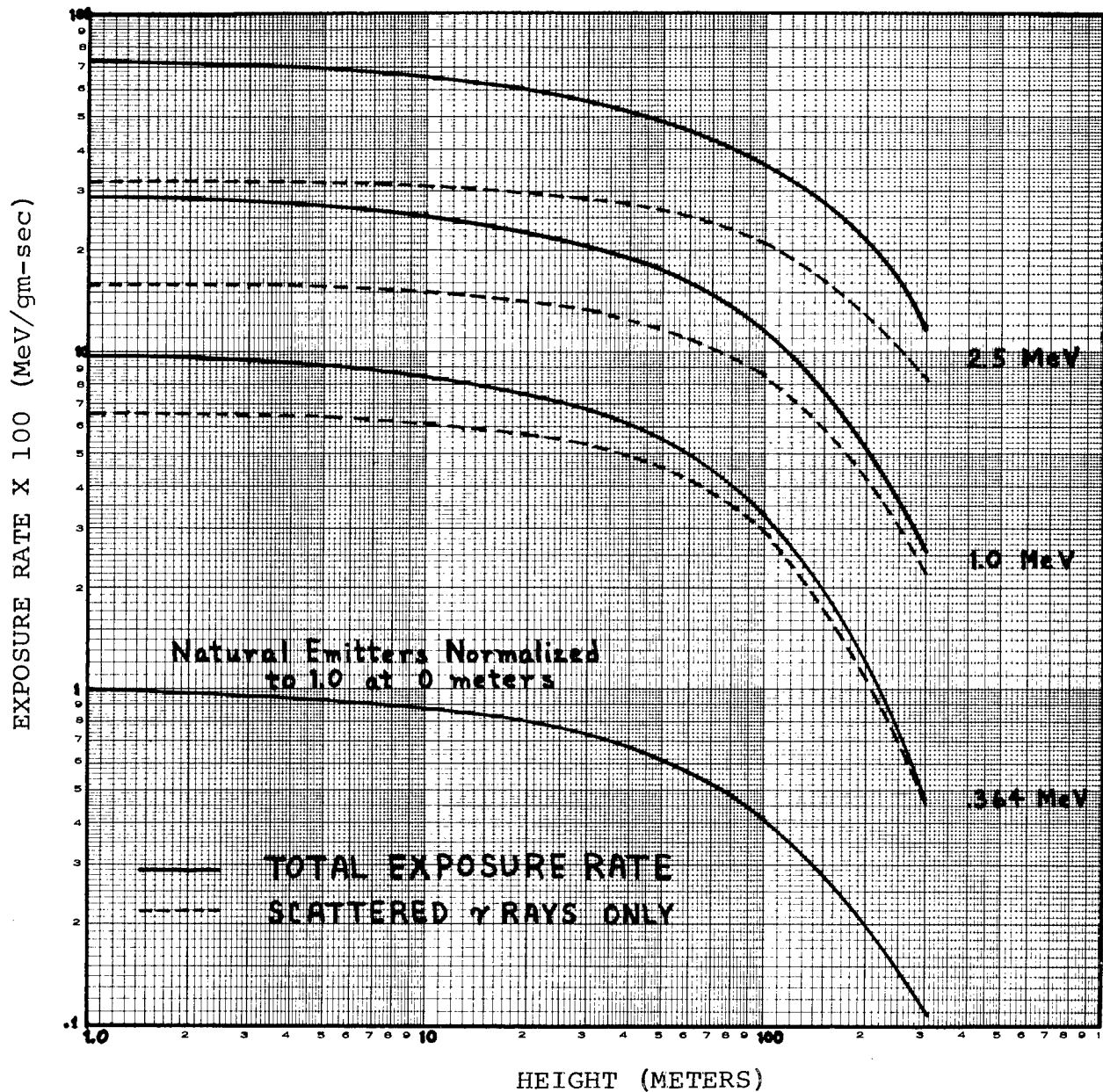


Figure 1. Total and scattered exposure rates versus height for uniformly distributed sources with energies of .364, 1.0 and 2.5 MeV and the single normalized curve of exposure rates for natural emitters.

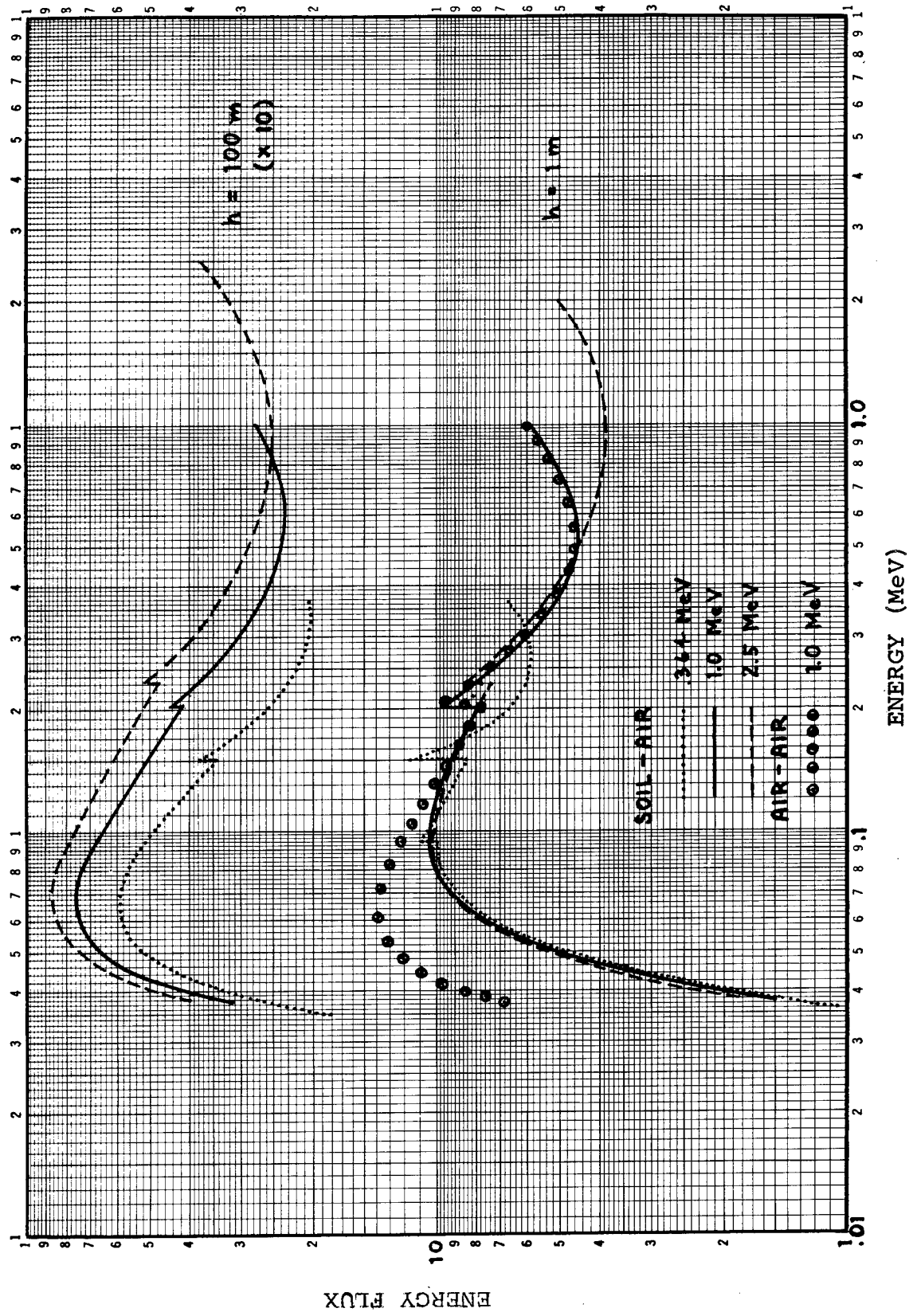


Figure 2. Differential energy spectra of the scattered energy flux (flux x energy) for three source energies at heights of 1 and 100 meters for a soil-air medium. Also shown for comparison, is the spectrum at 1 meter for a 1 Mev source in an infinite air medium.

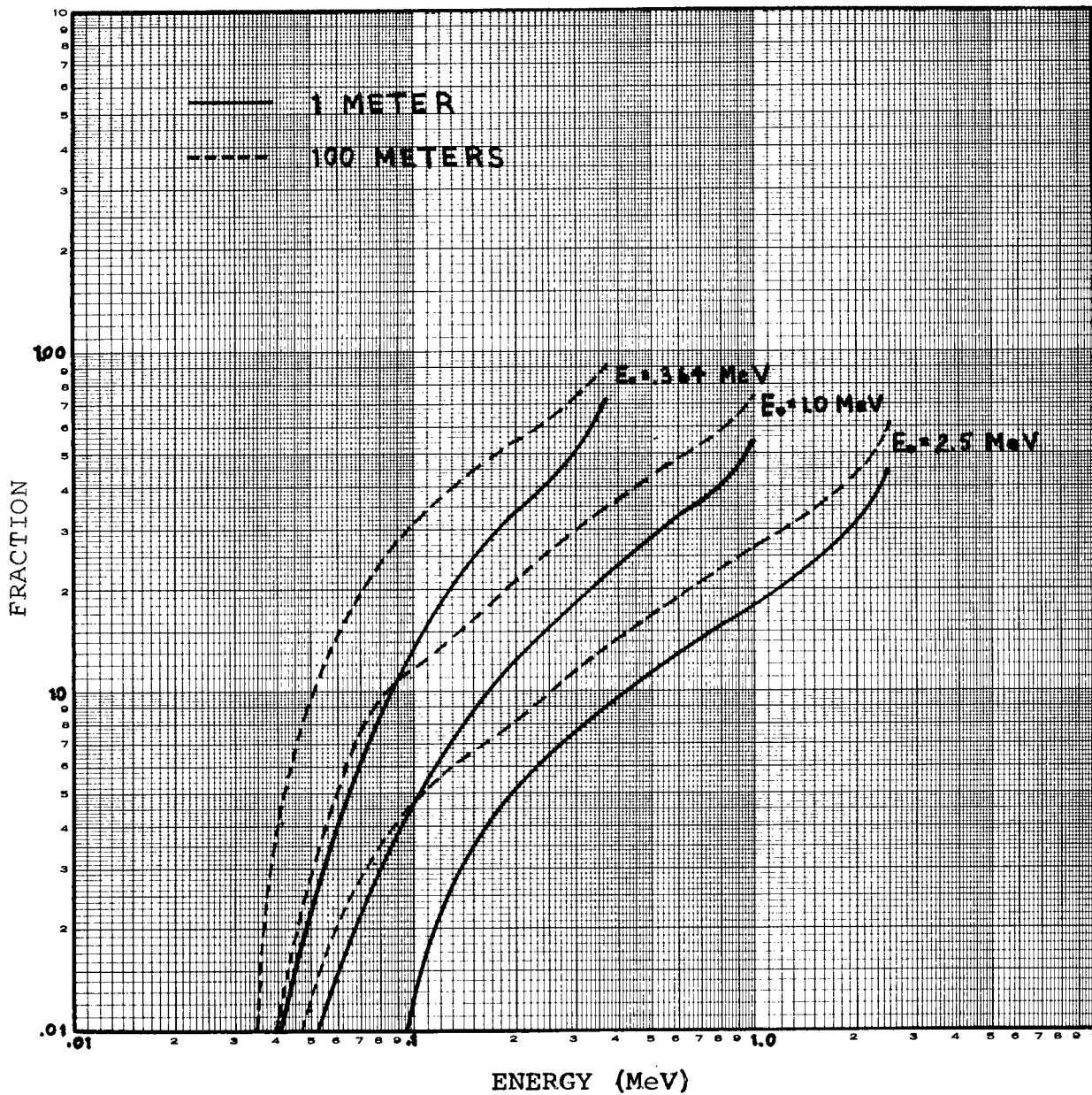


Figure 3. Integral exposure rate spectra (fraction of the total exposure rate due to gamma-rays of energy less than  $E$ ) at 1 and 100 meters for uniformly distributed sources.

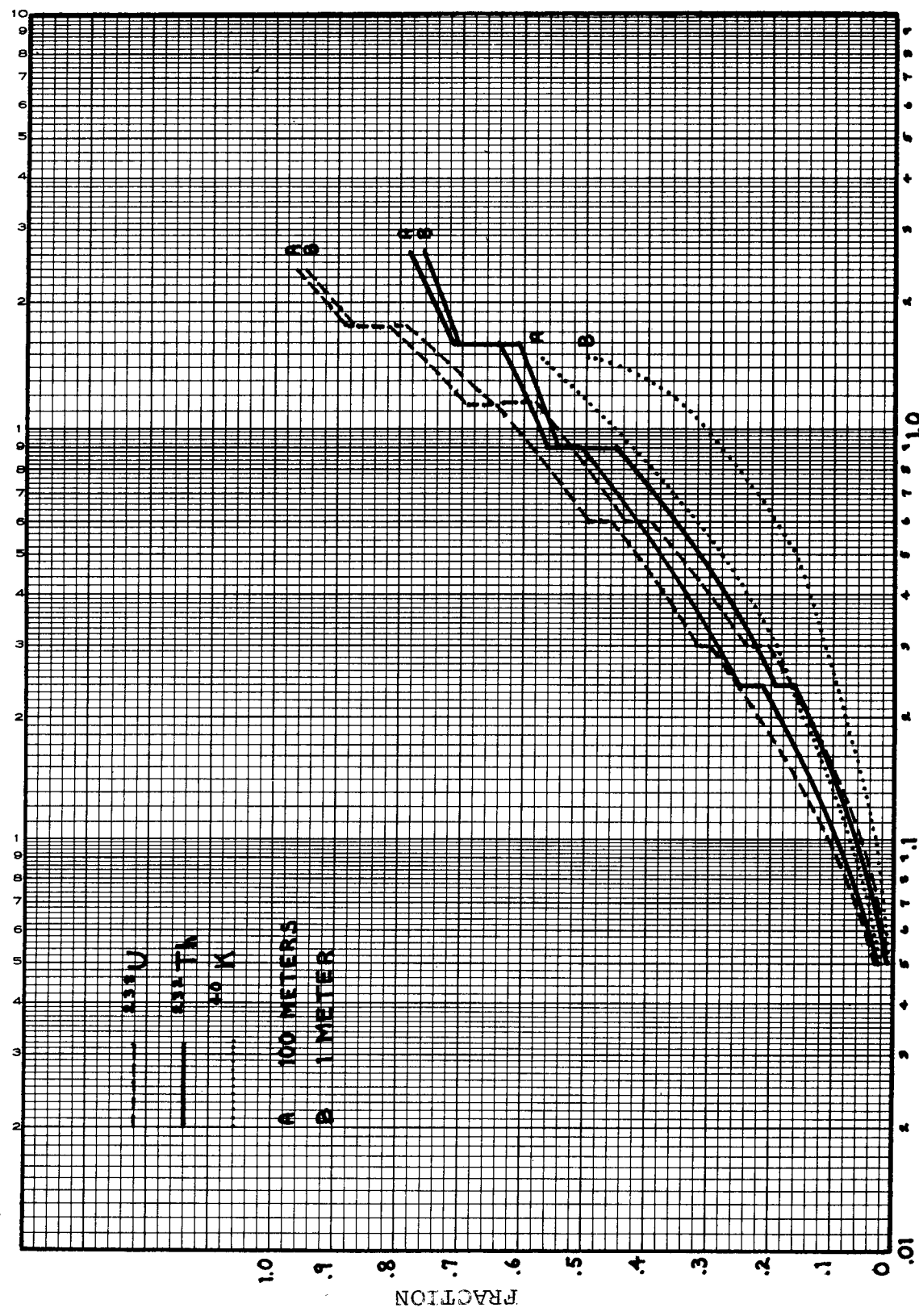


Figure 4. Integral exposure rate spectra (fraction of the total exposure rate due to gamma-rays of energy less than  $E$ ) for the natural emitters  $^{87}\text{Rb}$ ,  $^{40}\text{K}$ , and  $^{238}\text{U}$ , at 1 and 100 meters for uniformly distributed sources.

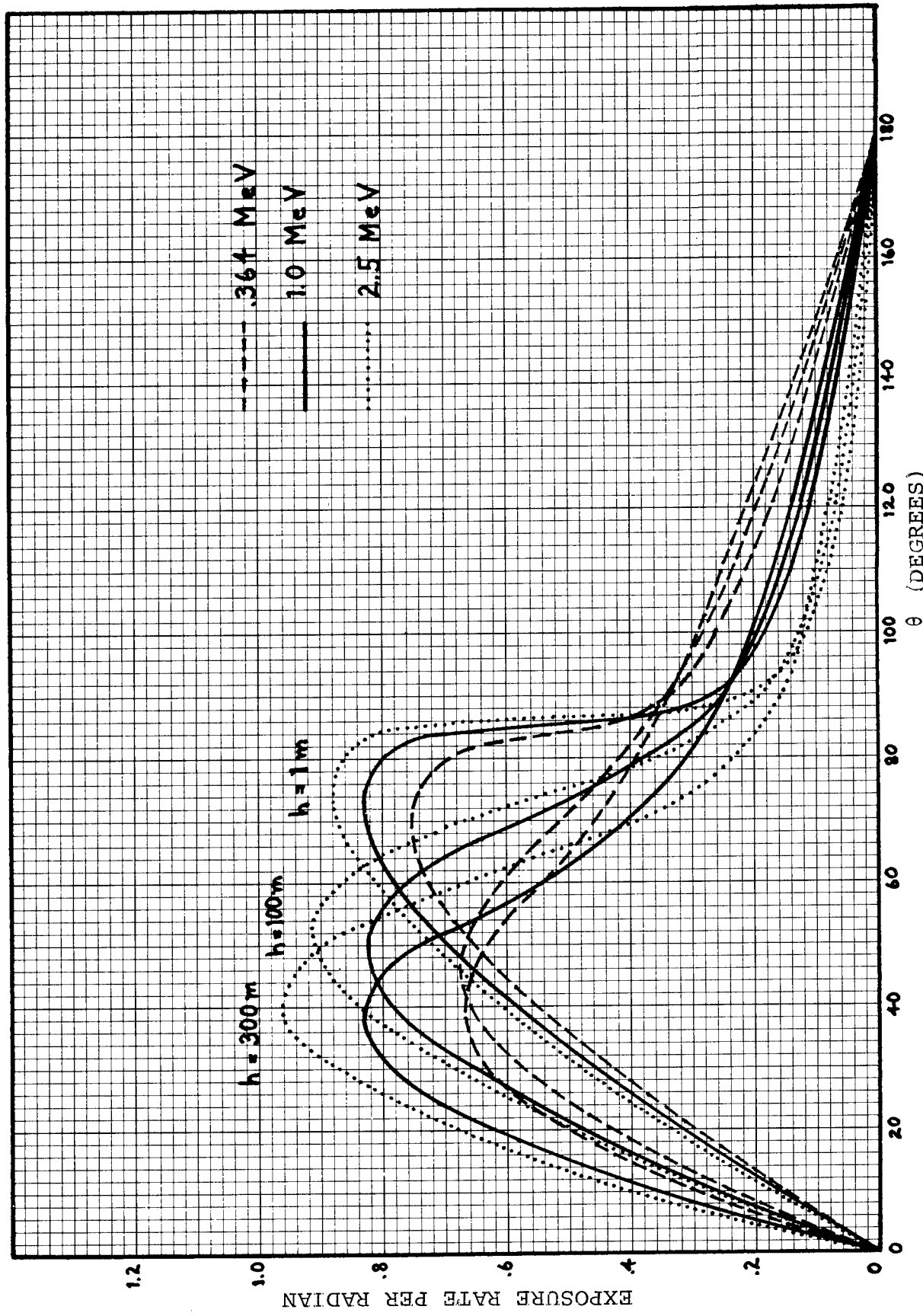


Figure 5. Differential angular exposure rate per radian (normalized to a total exposure rate of 1.0) at 1, 100, and 300 meters for uniformly distributed sources.

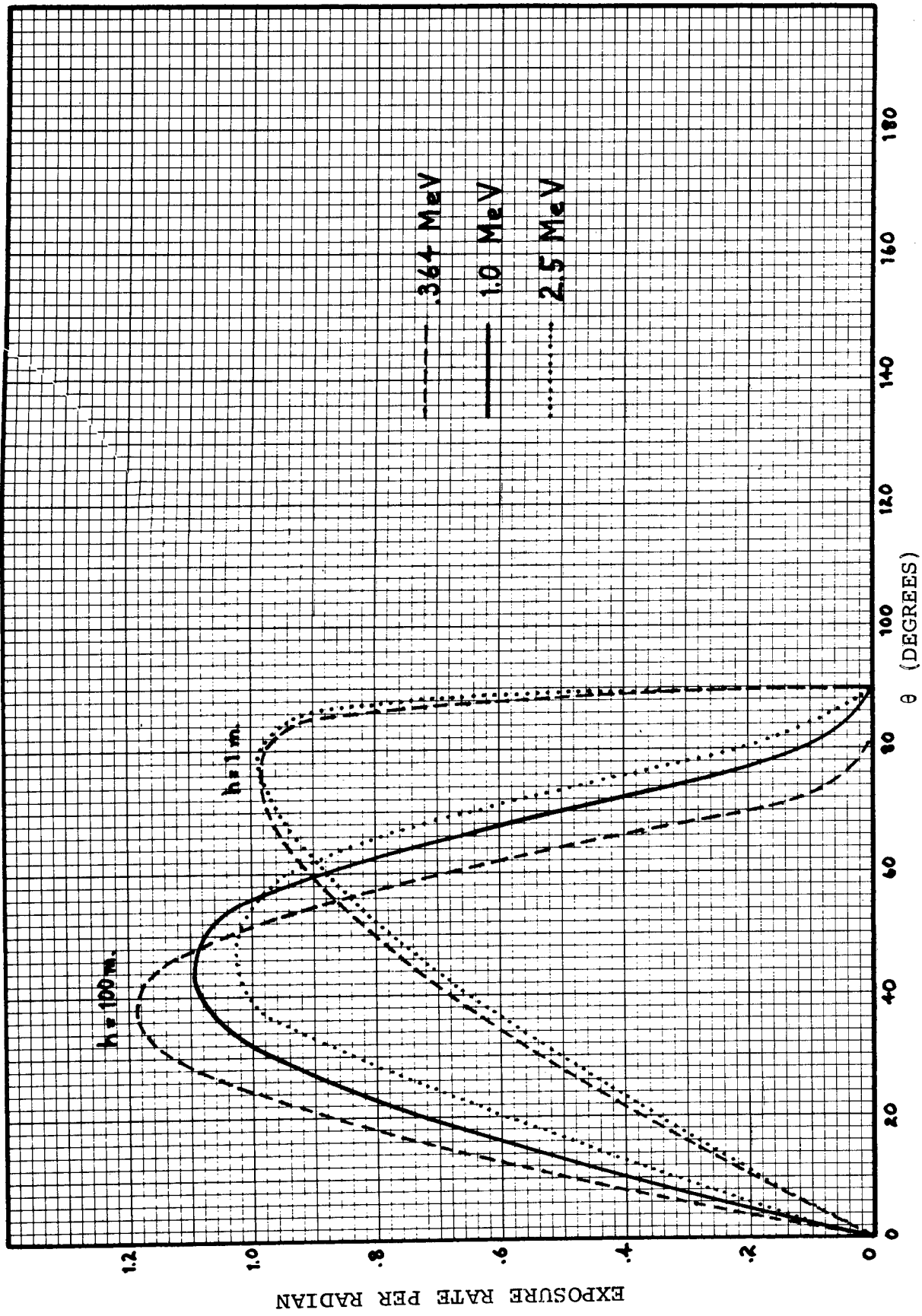


Figure 6. Differential angular exposure rate per radian for unscattered gamma-rays only (normalized to unscattered exposure rate of 1.0) at 1 and 100 meters uniformly distributed sources.

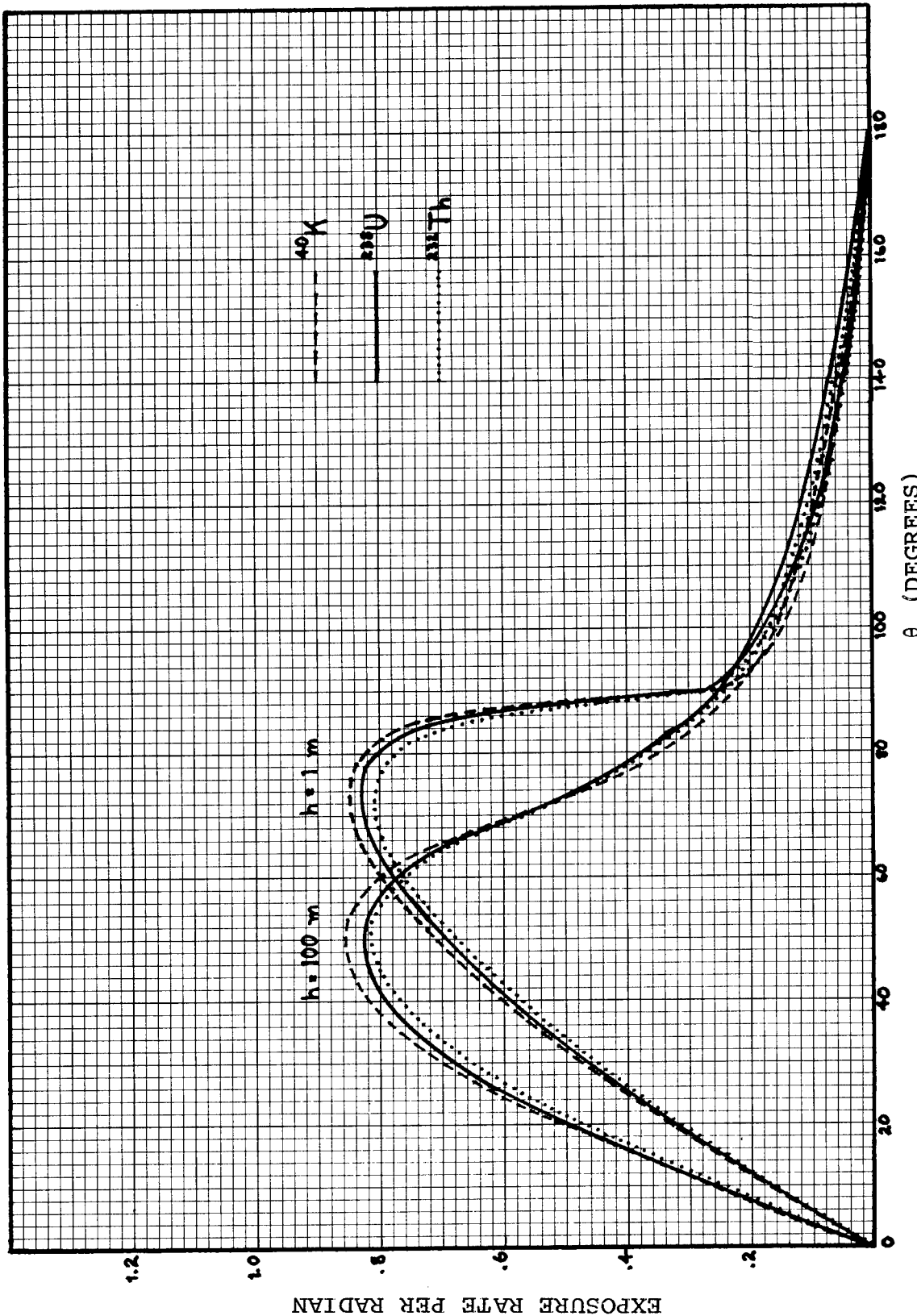


Figure 7. Differential angular exposure rate per radian for natural emitters normalized to a total exposure rate of 1) at 1 and 100 meters.

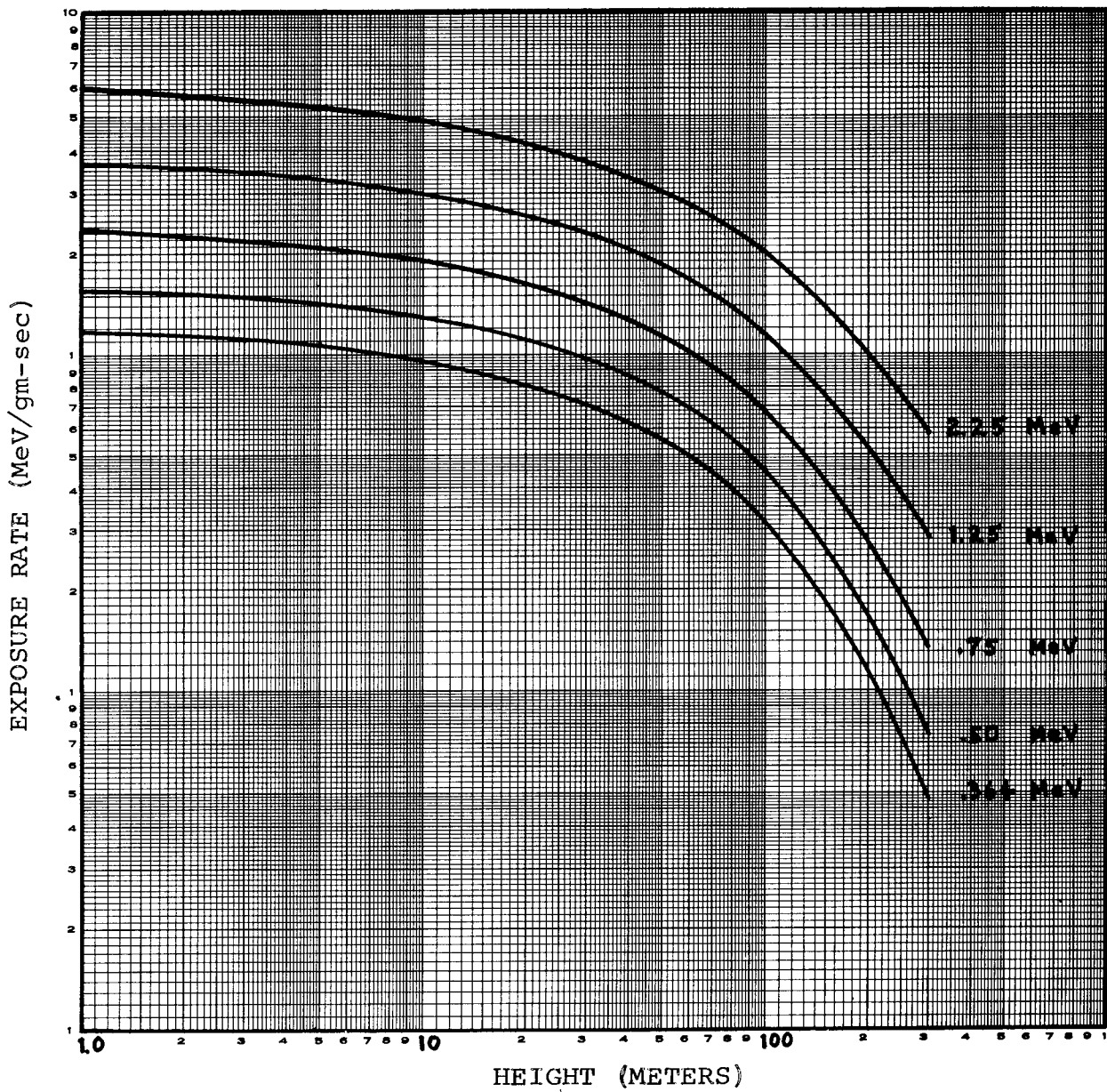


Figure 8. Total exposure rate for an exponentially distributed source ( $\alpha = .33$ ) for various source energies as a function of height.

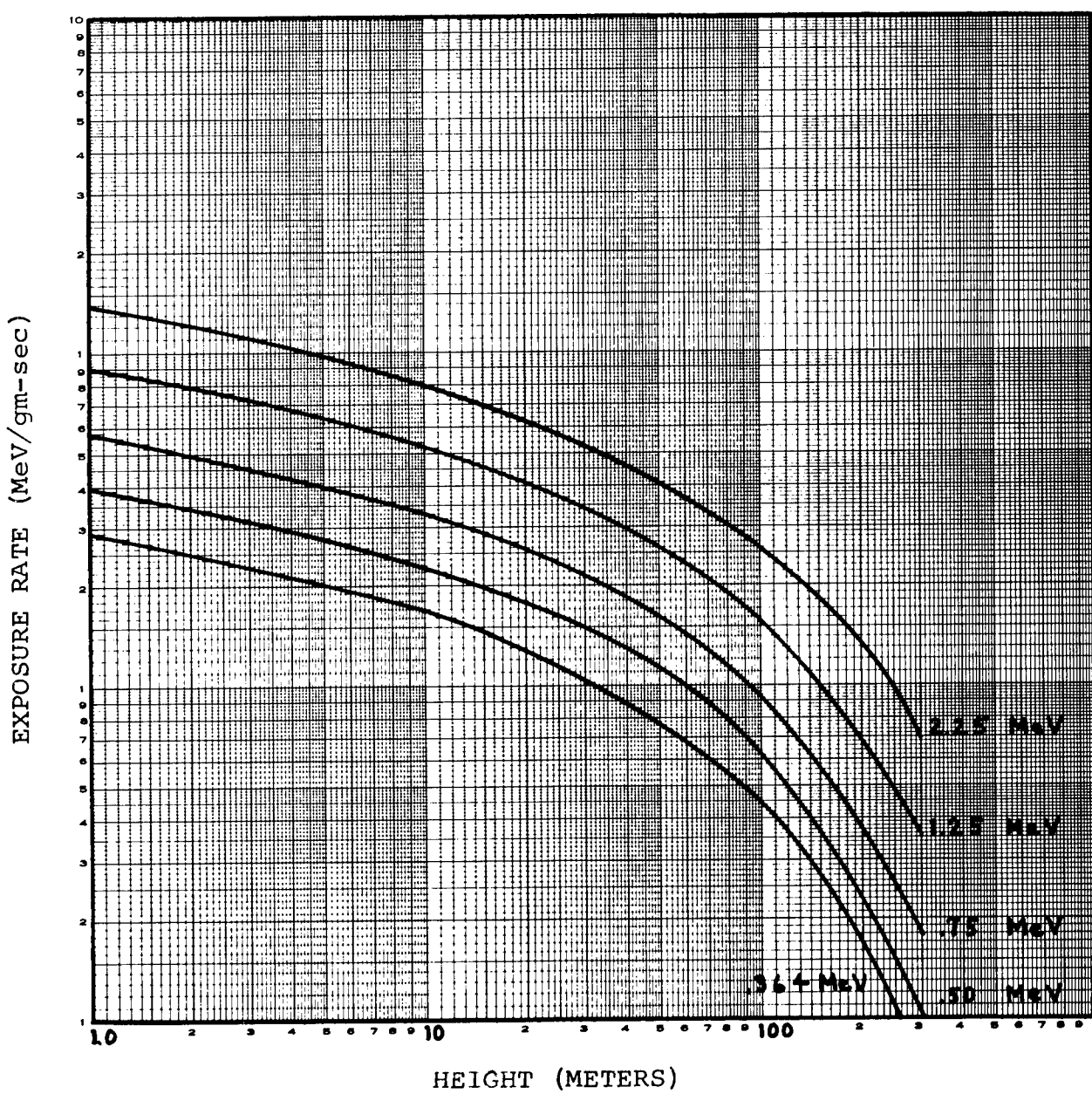


Figure 9. Total exposure rate for plane sources of various energies as a function of height.

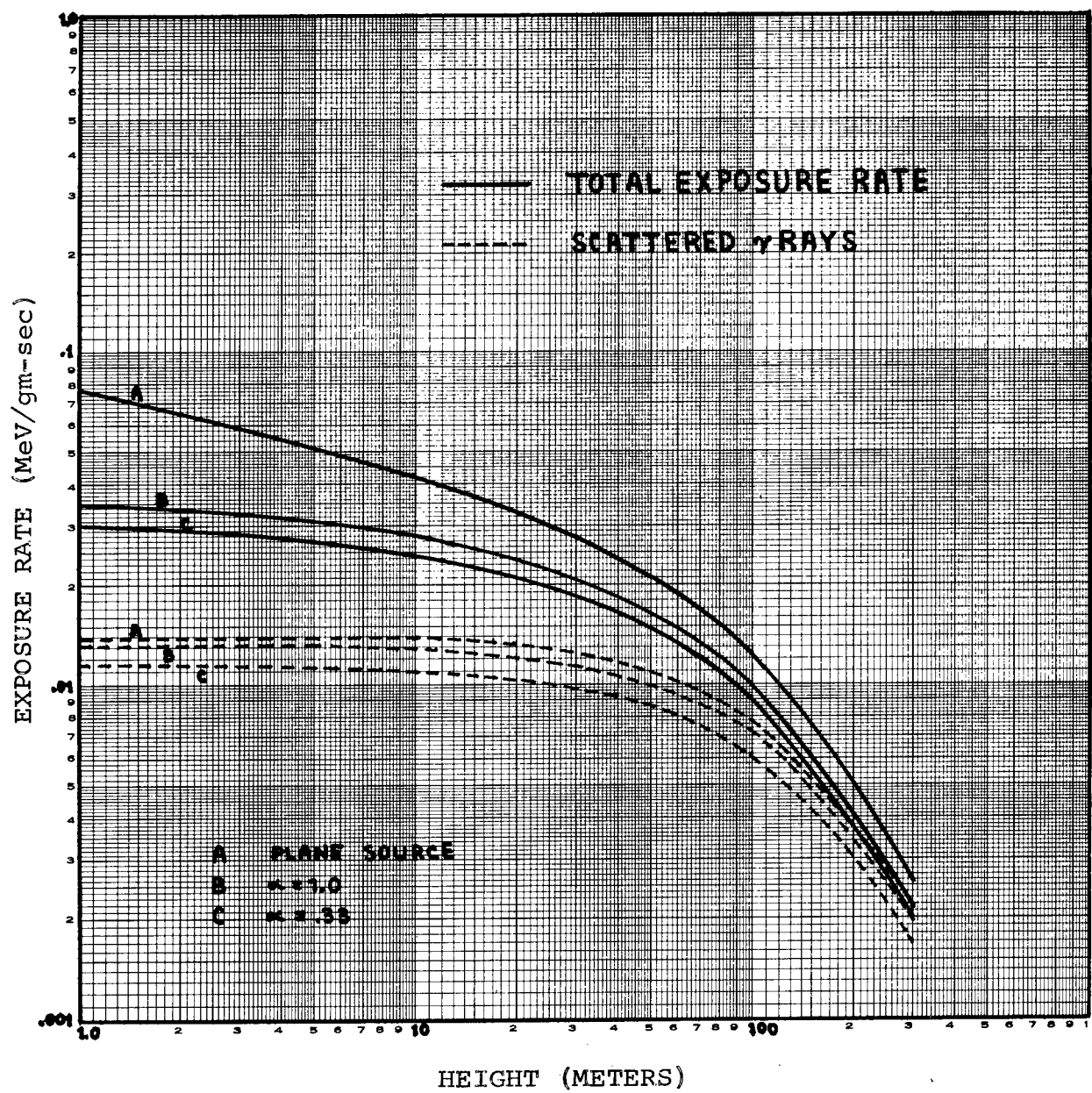


Figure 10. Total and scattered exposure rates as a function of height for various exponentially distributed sources, energy = 1 MeV.

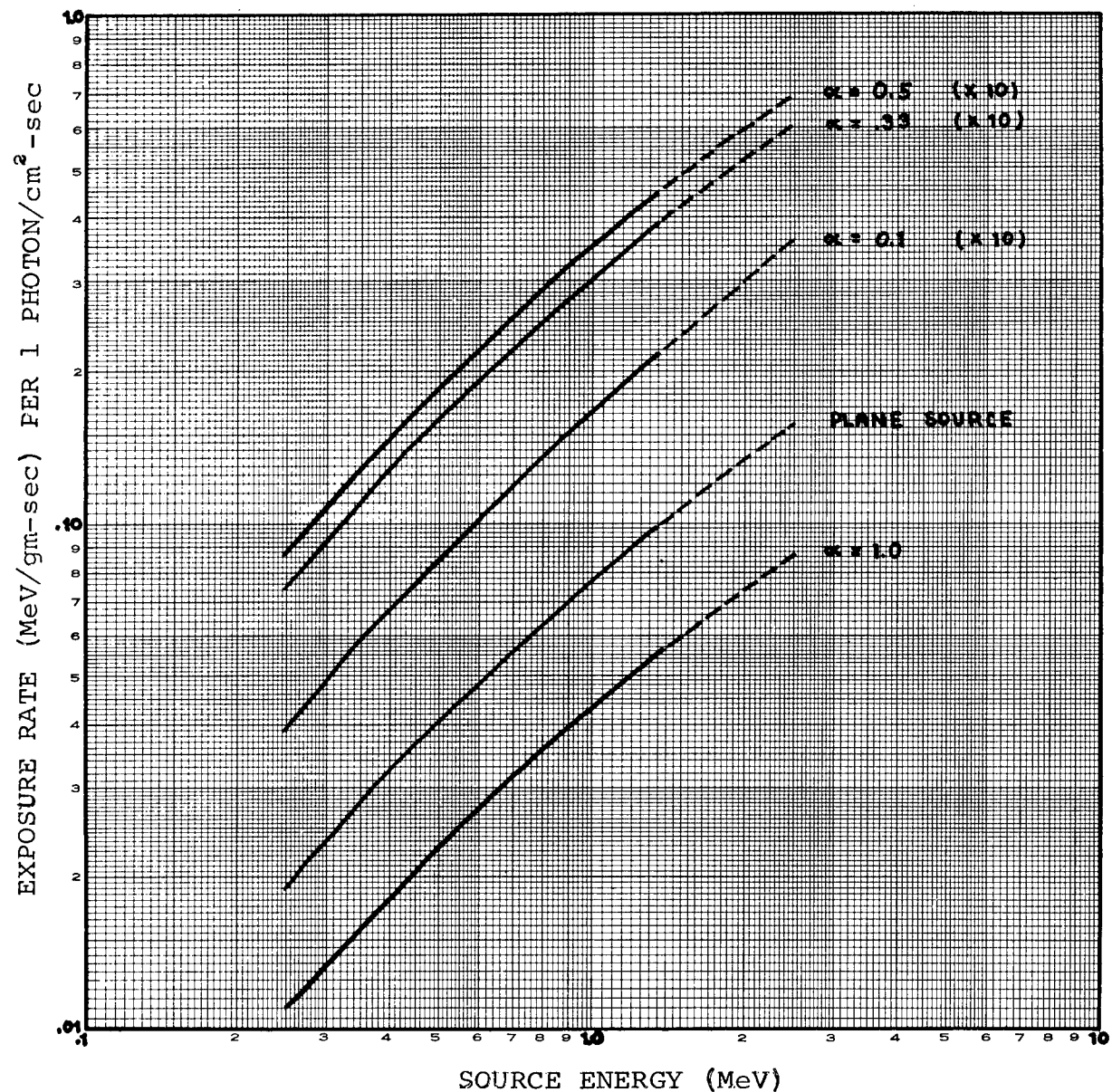


Figure 11. Total exposure rate as a function of energy at 1 meter for various depth distributions.

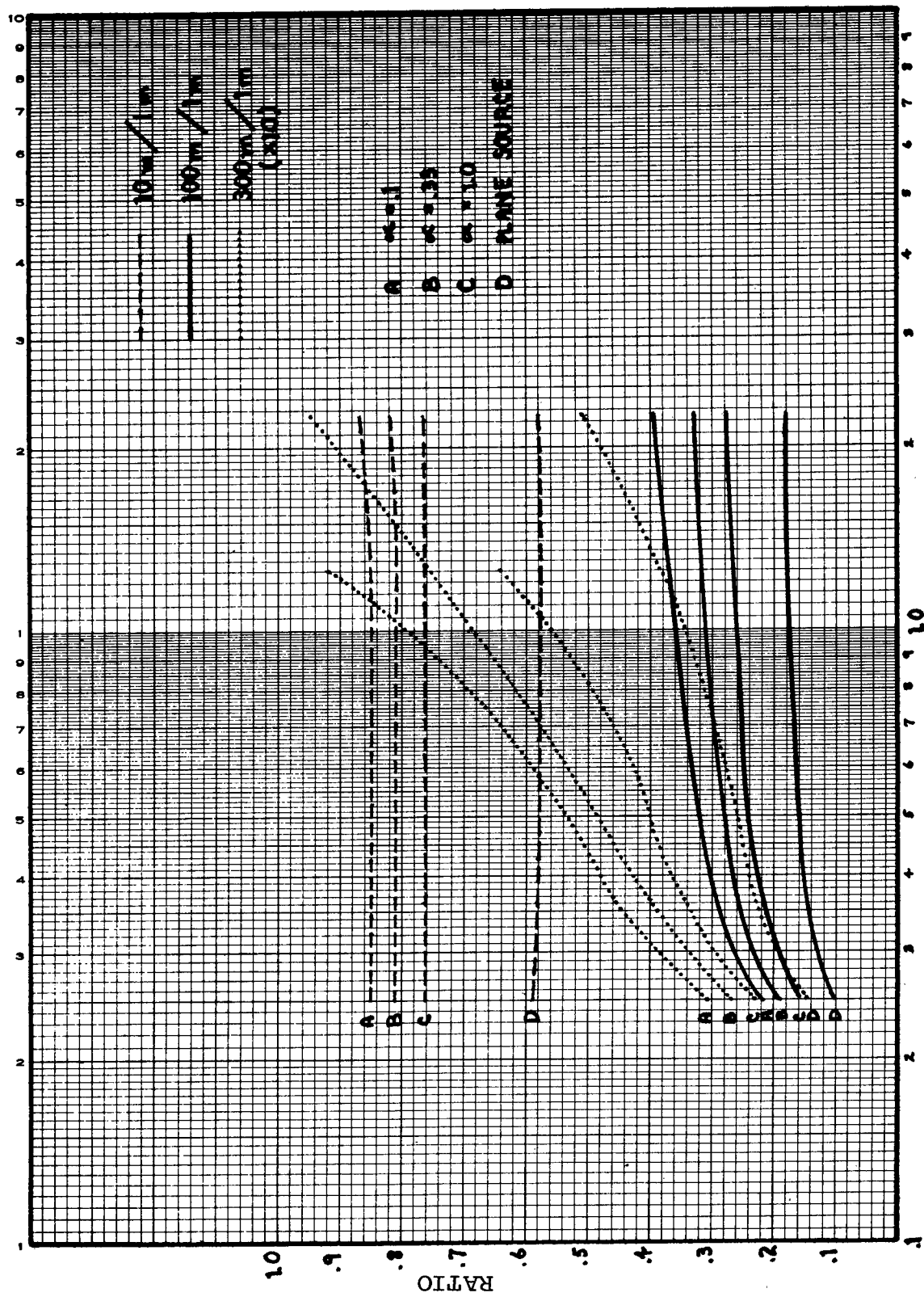


Figure 12. Effect of source depth distribution on total exposure rate at 10, 100, and 300 meters, relative to the total exposure rate at 1 meter.

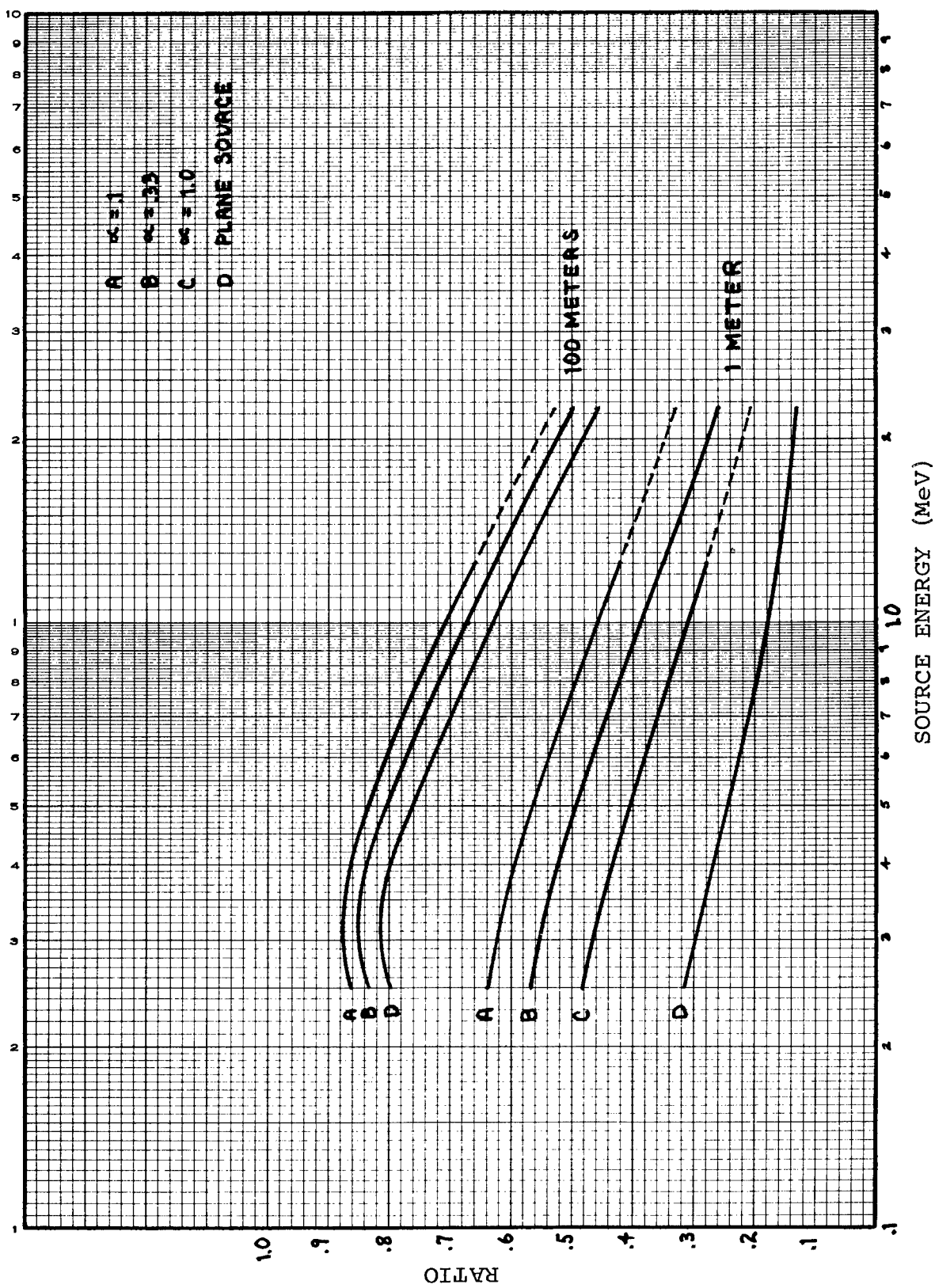


Figure 13. The ratio of the exposure rate due to scattered gamma-rays to total exposure rate at 1 and 100 meters for various depth distributions as a function of source energy.

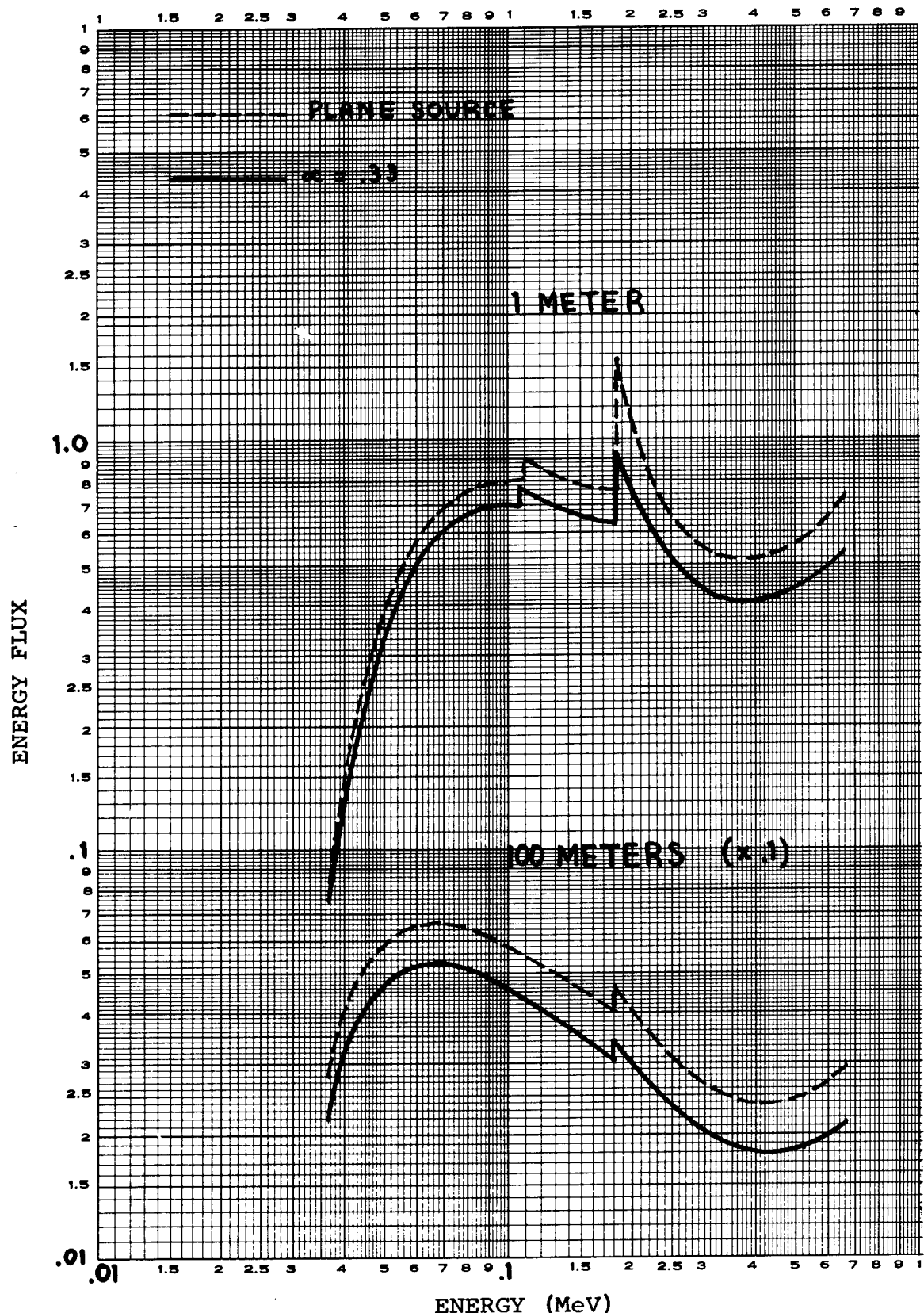


Figure 14. Differential energy spectra of the scattered energy flux at 1 and 100 meters for a .662 MeV source ( $^{137}\text{Cs}$ ).

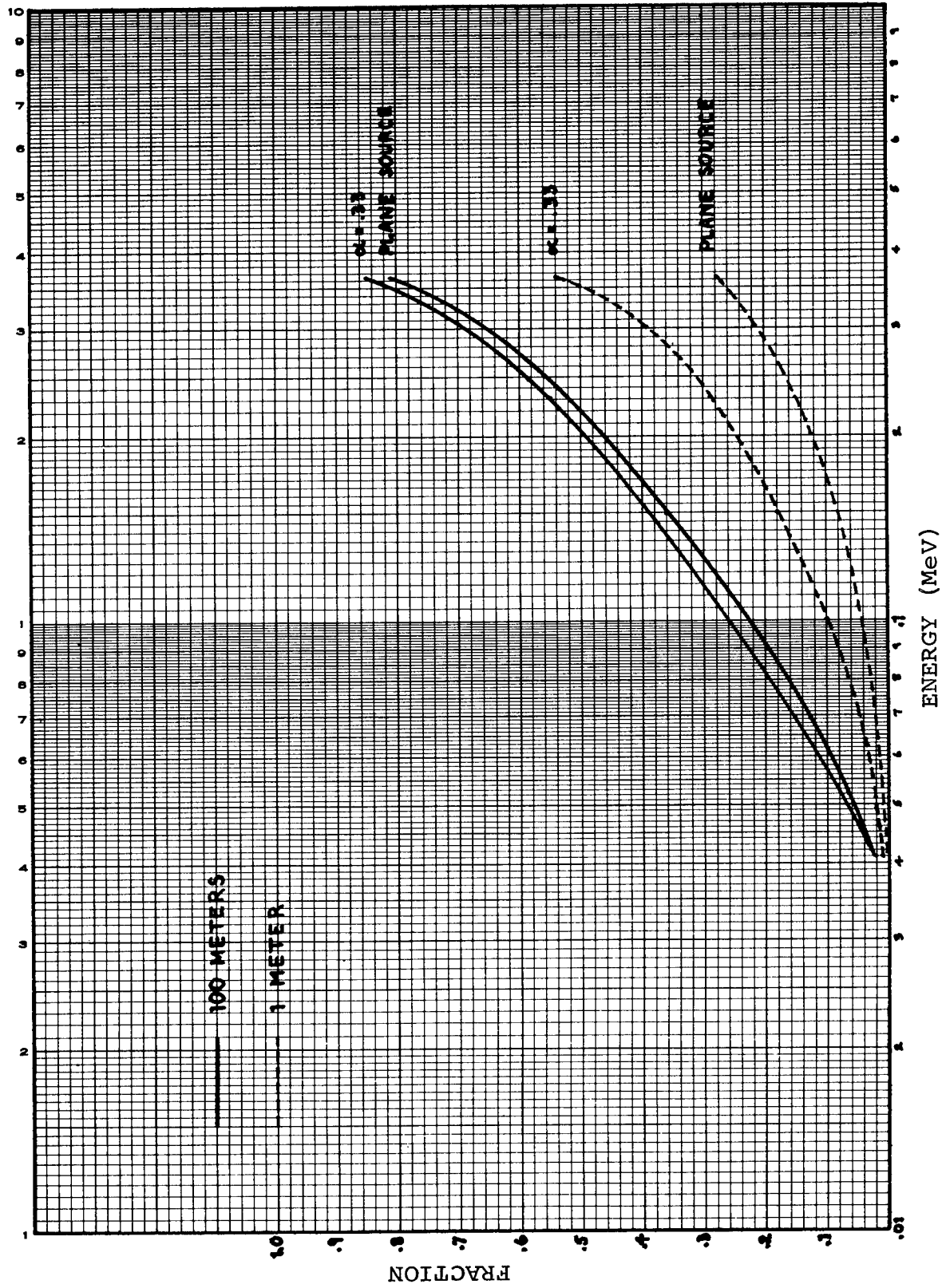


Figure 15. Integral exposure rate spectra (Fraction of total exposure rate due to gamma-rays of energy less than E) for a .364 MeV source at 1 and 100 meters.

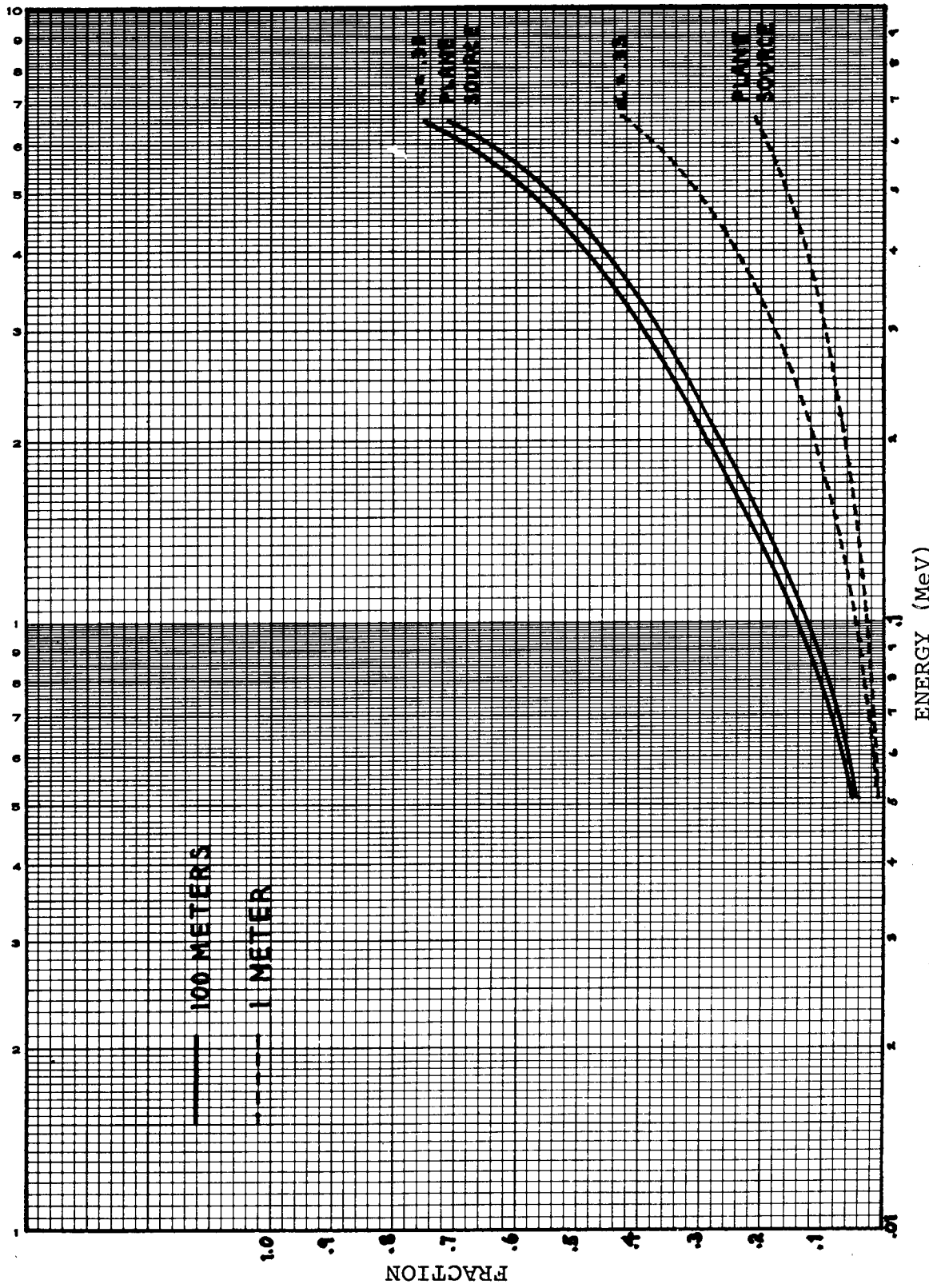


Figure 16. Integral exposure rate spectra (fraction of total exposure rate due to gamma-rays of energy less than E) for a .662 MeV source at 1 and 100 meters.

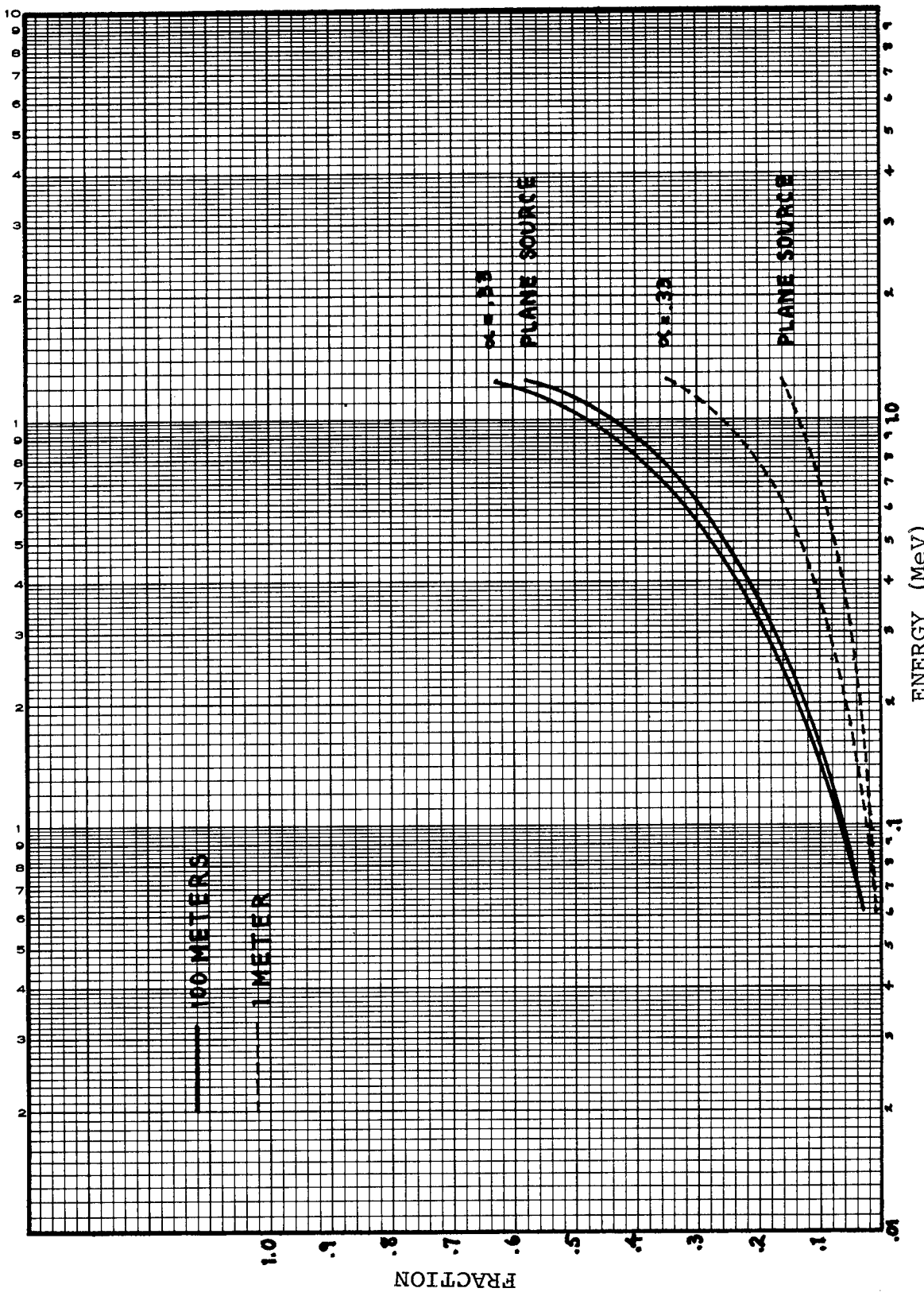


Figure 17. Integral exposure rate spectra (fraction of total exposure rate due to gamma-rays of energy less than  $E$ ) for a 1.25 MeV source at 1 and 100 meters.

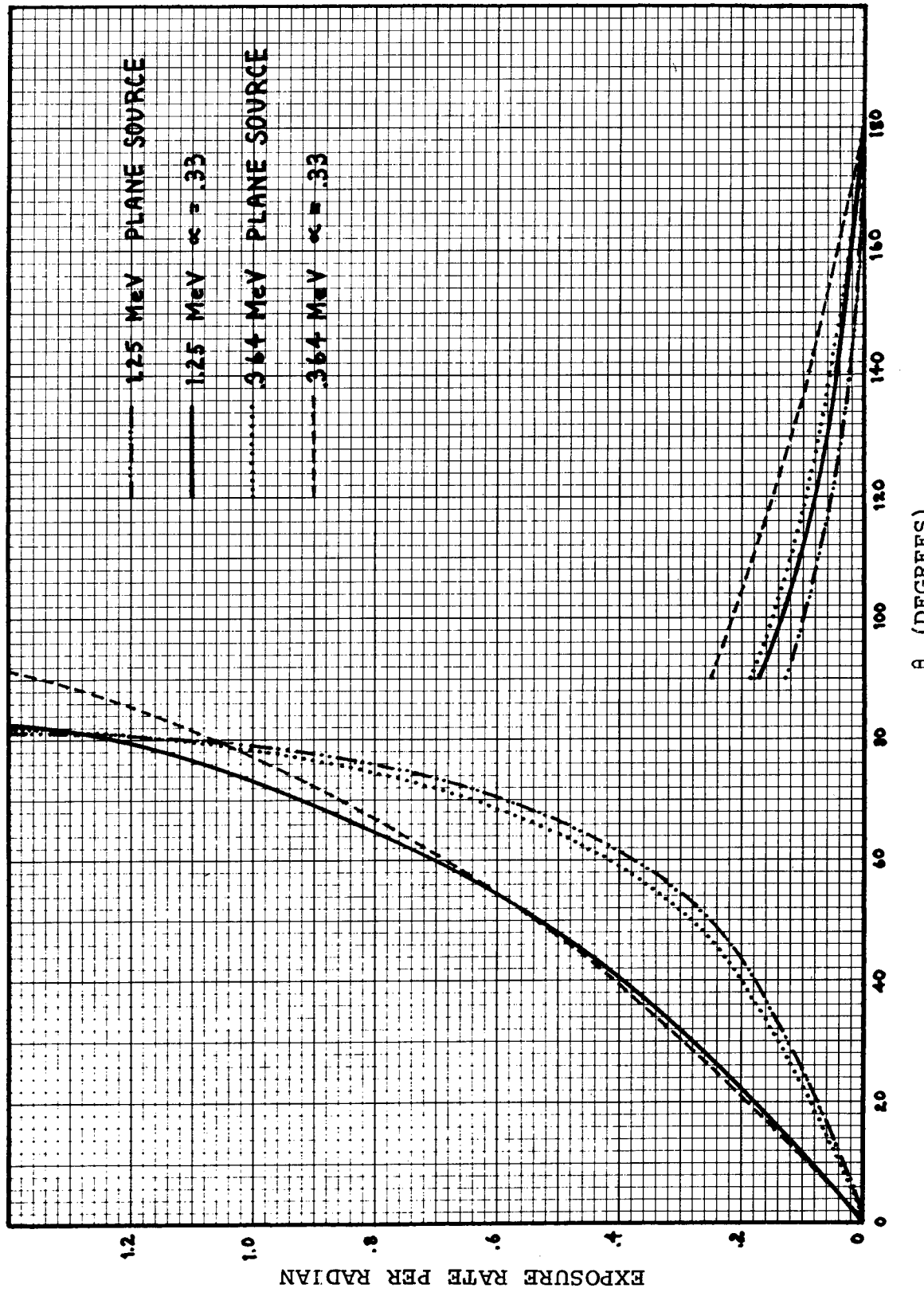


Figure 18a. Differential angular exposure rate distributions for plane and exponentially distributed sources at 1 meter (normalized to a total exposure rate of 1.0).

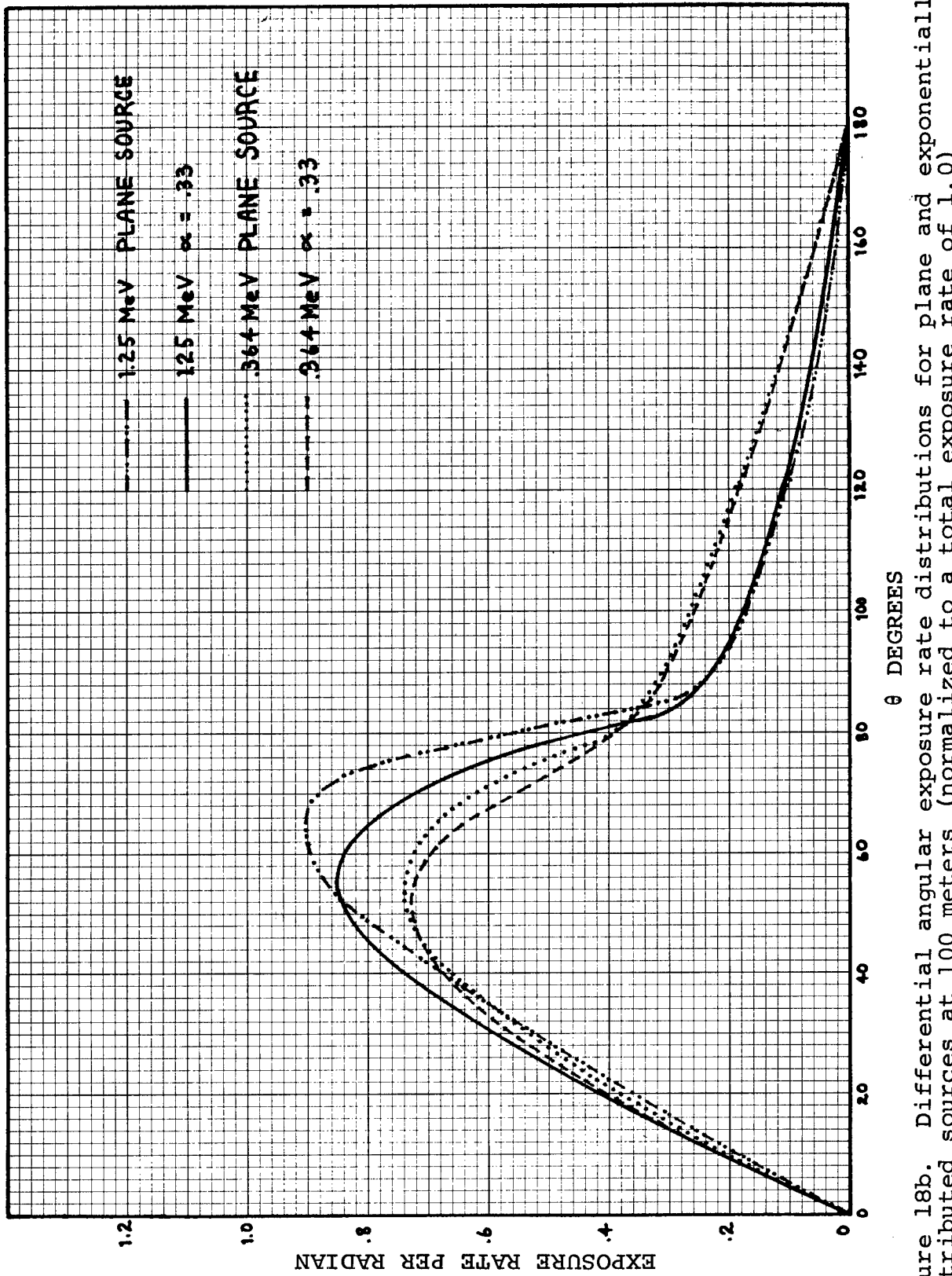


Figure 18b. Differential angular exposure rate distributions for plane and exponentially distributed sources at 100 meters (normalized to a total exposure rate of 1.0)